Neutron-poor nickel isotope anomalies in meteorites

Robert C. J. Steele[1,2,3]

r.steele@uclmail.net

and

Christopher D. Coath[1]

and

Marcel Regelous[1,4]

and

Sara Russell[2]

and

Tim Elliott[1]

ABSTRACT

We present new, mass-independent, Ni isotope data for a range of bulk chondritic meteorites. The data are reported as $\varepsilon^{60}Ni_{\frac{58}{61}}$, $\varepsilon^{62}Ni_{\frac{58}{61}}$ and $\varepsilon^{64}Ni_{\frac{58}{61}}$ or the parts per ten thousand deviations from a terrestrial reference, the NIST SRM 986 standard, of the $^{58}Ni/^{61}Ni$ internally normalised $^{60}Ni/^{61}Ni$, $^{62}Ni/^{61}Ni$ and $^{64}Ni/^{61}Ni$ ratios. The chondrites show a range of 0.15, 0.29 and 0.84 in $\varepsilon^{60}Ni_{\frac{58}{61}}$, $\varepsilon^{62}Ni_{\frac{58}{61}}$ and $\varepsilon^{64}Ni_{\frac{58}{61}}$ relative to a typical sample precision of 0.03, 0.05 and 0.08 (2 s.e.), respectively. The carbonaceous chondrites show the largest positive

[1]Bristol Isotope Group, School of Earth Sciences, University of Bristol, Wills Memorial Building, Queen's Road, Bristol, BS8 1RJ, UK

[2]Meteoritics and Cosmic mineralogy, The Natural History Museum, Cromwell Road, London, SW7 5BD, UK

[3]Now at: Department of Earth and Space Sciences, University of California Los Angeles (UCLA), Los Angeles, CA 90095–1567, USA

[4]Now at: GeoZentrum Nordbayern, Universität Erlangen-Nürnberg, Schlossgarten 5, D-91054 Erlangen, Germany

anomalies, enstatite chondrites have approximately terrestrial ratios, though only EH match Earth's composition within uncertainty, and ordinary chondrites show negative anomalies. The meteorite data show a strong positive correlation between $\varepsilon^{62}Ni_{\frac{58}{61}}$ and $\varepsilon^{64}Ni_{\frac{58}{61}}$, an extrapolation of which is within error of the average of previous measurements of CAIs. Moreover, the slope of this bulk meteorite array is 3.003 ±0.166 which is within error of that expected for an anomaly solely on ^{58}Ni. We also determined to high precision (∼10 ppm per AMU) the mass-dependent fractionation of two meteorite samples which span the range of $\varepsilon^{62}Ni_{\frac{58}{61}}$ and $\varepsilon^{64}Ni_{\frac{58}{61}}$. These analyses show that 'absolute' ratios of ^{58}Ni/^{61}Ni vary between these two samples whereas those of ^{62}Ni/^{61}Ni and ^{64}Ni/^{61}Ni do not. Thus Ni isotopic differences seem most likely explained by variability in the neutron-poor ^{58}Ni, and not correlated anomalies in the neutron-rich isotopes, ^{62}Ni and ^{64}Ni. This contrasts with previous inferences from mass-independent measurements of Ni and other transition elements which invoked variable contributions of a neutron-rich component. We have examined different nucleosynthetic environments to determine the possible source of the anomalous material responsible for the isotopic variations observed in Ni and other transition elements within bulk samples. We find that the Ni isotopic variability of the Solar System cannot be explained by mixing with a component of bulk stellar ejecta from either SN II, Wolf Rayet nor AGB source and is unlikely to result from bulk mixing of material from an SN Ia. However, variable admixture of material from the Si/S zone of an SN II can create all the characteristics of Ni isotope variations in Solar System materials. Moreover, these characteristics can also be provided by an SN II with a range of masses from 15 to 40 $M_{\odot}$ showing input from SN II is a robust source for Ni isotope variations in the Solar System. Correlations of Ni isotope anomalies with O, Cr and Ti isotope ratios and Pb/Yb in bulk meteorites suggests that the heterogeneous distribution of isotopic anomalies in the early Solar System likely resulted from nebular sorting of chemically or physically different materials bearing different amounts of isotopes synthesised proximally to the collapse of the proto-solar nebula.

Subject headings: Nickel, Mass-independent, Isotopes, Early Solar System

1. Introduction

The discovery of isotopic anomalies in neutron-rich isotopes of Ca (Lee et al. 1978; Jungck et al. 1984) and iron group elements, e.g. Ti (Heydegger et al. 1979; Niemeyer and Lugmair 1980; Niederer et al. 1980) in calcium, aluminium rich inclusions (CAIs), was interpreted as strong evidence of heterogeneous input to the early Solar System of material from a highly neutron enriched supernova source. However, debate over the origin and circumstances of this event has continued and been added to by the discovery of mass-independent anomalies in bulk samples as well as CAIs. The progenitor of this neutron-rich component has been hypothesised to be type Ia supernova (SN Ia) (e.g. Nomoto 1982; Hartmann et al. 1985; Meyer et al. 1996; Woosley 1997), type II supernova (SN II) (e.g. Hartmann et al. 1985) or an asymptotic giant branch star (AGB) (e.g. Lugaro et al. 2004). It is likely that the source of the isotopic heterogeneity observed in early Solar System materials is derived from the most recent nucleosynthetic event and therefore this heterogeneity may contain information about the birth environment of the Sun.

When attempting to identify sources of isotopic heterogeneity in the Solar System, an important consideration resulting from the greatly differing isotopic compositions produced in different nucleosynthetic environments is the need to consider the possibility of effects on all the isotopes of the studied element. The majority of isotopic anomalies in meteorites are reported as mass-independent ratios which are normalised to an isotope ratio thought not to contain anomalies. This normalisation removes the effects of mass-dependent fractionation, both natural and instrumental, which otherwise obscure potentially subtle source related anomalies. However, the highly anomalous isotope ratios produced by stellar nucleosynthesis are not necessarily limited to a single isotope. Moreover, for some elements the choice of normalising isotopes has been influenced by the assumption of neutron-rich isotope anomalies (e.g. Birck and Lugmair 1988). This makes the existence of anomalies on neutron-rich isotopes a point of interpretation as they may equally reside on the neutron-poor isotopes. This problem can be tackled in two ways. First and most obvious is to determine the location of anomalies by determining the 'absolute' isotope ratios (e.g. Niederer et al. 1985). Where only small anomalies exist, such as in bulk samples, this may be very analytically challenging. The second approach is to consider nucleosynthetic contributions to all isotopes without making the assumption that any one ratio is unaffected. In these two ways robust information about the nucleosynthetic origins of the Solar System can be obtained from isotopic analyses of early Solar System materials.

As an iron group element Ni has a relatively high abundance in the Solar System. It also exhibits moderately refractory, moderately siderophile, behaviour and so is a major constituent of most meteorites. Nickel has five stable isotopes which are produced with contrasting efficiencies in different nucleosynthetic environments, so may provide valuable constraints on the stellar sources of the Solar System. Moreover, two of the isotopes, ^{62}Ni and ^{64}Ni, are highly neutron-rich and so offer a good test of hypothesised input to the Solar System from a high neutron density SN Ia (e.g. Nomoto 1982; Hartmann et al. 1985; Meyer et al. 1996; Woosley 1997). Nickel also has enough isotopes that the mass-dependent fractionation of samples can be determined by double spike analysis, meaning it may be possible to determine on which isotopes the anomalies reside. One isotope, ^{60}Ni, is the decay product of the short-lived ^{60}Fe ($t_{1/2}$ = 2.62Ma, Rugel et al. 2009), so Ni isotope measurements of meteorites may also provide a constraint for the short-lived radionuclide (SLR) budget of the early Solar System. Therefore, Ni offers a tempting opportunity to study the nucleosynthetic sources of the materials that make up the Solar System and how they were mixed in its earliest history.

2. Results

Nickel isotope data from suite of 7 carbonaceous chondrites, 3 enstatite chondrites and 7 ordinary chondrites are presented, see Table 1. The methods used to collect these data are outlined in the appendix and Steele et al. (2011). These data comprise measurements on both fully processed samples and previously separated Ni splits (Regelous et al. 2008) that have undergone additional processing to remove Zn for high precision determination of ^{64}Ni. The data show a range of 0.16, 0.29 and 0.84 ‰ in $\varepsilon^{60}\mathrm{Ni}_{\frac{58}{61}}$, $\varepsilon^{62}\mathrm{Ni}_{\frac{58}{61}}$ and $\varepsilon^{64}\mathrm{Ni}_{\frac{58}{61}}$, respectively, where $\varepsilon^{i}\mathrm{Ni}_{\frac{58}{61}}$ is the parts per ten thousand (‰) difference in the ^{i}Ni/^{61}Ni ratio, internally normalised to ^{58}Ni/^{61}Ni, relative to the NIST SRM 986 standard. There is a strong positive correlation between $\varepsilon^{62}\mathrm{Ni}_{\frac{58}{61}}$ and $\varepsilon^{64}\mathrm{Ni}_{\frac{58}{61}}$, Figure 1, which overlaps that previously defined by measurements of iron meteorites (Steele et al. 2011). The combined datasets yield a slope of 3.003 ±0.166 (MSWD = 1.021, n = 215). This slope, uncertainty and MSWD were determined by York regression (York 1969; Mahon 1996; York et al. 2004) using all 215 individual analyses of all 30 meteorite and peridotite samples, including iron meteorites from Steele et al. (2011). Tlacotepec was not used as it shows evidence of spallation (Steele et al. 2011). Uncertainties used in the regression were estimated from the entire dataset (by the method de-

	Group	NHM no.	n	n_{64}	$\varepsilon^{60}Ni_{\frac{58}{61}}$	2 s.e.	$\varepsilon^{62}Ni_{\frac{58}{61}}$	2 s.e.	$\varepsilon^{64}Ni_{\frac{58}{61}}$	2 s.e.	$\delta^{60/58}Ni$	2 s.e.
Carbonaceous Chondrites												
Orgueil^{+}	CI	1985, M148	4	4	-0.008	0.010	0.203	0.031	0.585	0.089	0.185	0.024
Leoville^{+}	CV	1919, 144	8	8	-0.107	0.011	0.061	0.028	0.135	0.076	0.300*	0.050
Allende^{+}	CV	—	4	4	-0.098	0.016	0.131	0.019	0.324	0.036	—	—
NWA-801^{+}	CR	—	5	5	-0.157	0.015	0.116	0.022	0.361	0.065	—	—
Felix^{+}	CO	1919, 89	4	4	-0.079	0.030	0.097	0.029	0.262	0.107	0.310*	0.070
Murchison^{+}	CM	1988, M23	4	4	-0.098	0.028	0.124	0.033	0.298	0.092	0.210*	0.030
Cold-Bokkeveld^{+}	CM	13989	4	4	-0.084	0.020	0.113	0.050	0.335	0.105	—	—
Ordinary Chondrite												
Dhurmsala	LL	—	4	4	-0.049	0.027	-0.085	0.011	-0.210	0.059	—	—
Chainpur^{+}	LL	1915, 86	8	8	-0.054	0.017	-0.065	0.036	-0.171	0.102	0.280*	0.100
Tieschitz^{+}	HL	1975, M11	8	8	-0.052	0.019	-0.080	0.036	-0.253	0.048	—	—
Tenham	L	—	4	4	-0.026	0.020	-0.057	0.025	-0.117	0.135	—	—
Barratta	L	—	4	4	-0.042	0.022	-0.028	0.027	-0.105	0.073	—	—
Ceniceros	H	—	4	4	-0.063	0.010	-0.050	0.028	-0.078	0.102	—	—
Butsura	H	—	28	28	-0.048	0.008	-0.053	0.014	-0.171	0.033	—	—
Enstatite Chondrite												
Khairpur^{+}	EL	51366	4	4	-0.023	0.023	-0.054	0.028	-0.049	0.064	—	—
St.Mark's^{+}	EH	1990, 339	4	4	-0.017	0.014	0.039	0.039	0.113	0.067	—	—
Abee^{+}	EH	992, M7	4	4	-0.007	0.023	0.027	0.058	0.084	0.071	0.190*	0.050
Terrestrial Standards												
NIST SRM 361	T	—	72	41	-0.011	0.007	0.029	0.013	0.136	0.033	-0.039	0.032
NIST SRM 986-col	T	—	4	4	0.002	0.006	-0.024	0.028	0.000	0.042	—	—
PtYG	T	—	20	20	0.010	0.008	-0.009	0.017	0.012	0.033	-0.645	0.080
JP-1	T	—	58	50	-0.006	0.007	0.035	0.010	0.117	0.021	0.100	0.080
DTS-2	T	—	4	4	-0.007	0.032	0.038	0.063	0.161	0.100	0.128	0.080
Bulk Silicate Earth	T	—	—	—	-0.006	0.007	0.036	0.010	0.119	0.021	0.179	0.036

Table 1: Table showing mass-dependent and mass-independent Ni isotope data, reported relative to NIST SRM 986, for chondrites and terrestrial materials. *Mass-dependent $\delta^{60/58}$Ni data published by Cameron et al. (2009). $^{+}$Meteorite samples dissolved and initially processed by Regelous et al. (2008); before analysis these solutions were passed through anionic exchange resin (see Steele et al. 2011) in order to remove residual Zn. NIST SRM 361 and JP-1 have been processed both by Regelous et al. (2008) and during this study. The estimate for the bulk silicate Earth (BSE) is taken from Steele et al. (2011).

scribed in Steele et al. 2011, and in the appendix) and give values of 0.042 and 0.082 ‰ (1 standard deviation (1 s.d.) on a single analysis, compared to the 2 s.e. for the averaged analyses for given samples reported in Table 1) for $\varepsilon^{62}Ni_{\frac{58}{61}}$ and $\varepsilon^{64}Ni_{\frac{58}{61}}$ respectively and correlation coefficient of 0.68. Numerical simulations showed these 215 'raw' data provided a more accurate slope than regressions using averages and standard errors, see appendix. Notably, an extrapolation of this best fit line intersects the compositions of the CAIs previously measured by Birck and Lugmair (1988), see Figure 2(a), suggesting a common process produces the Ni isotopic variations in CAIs and bulk meteorites (see also, Trinquier et al. 2009).

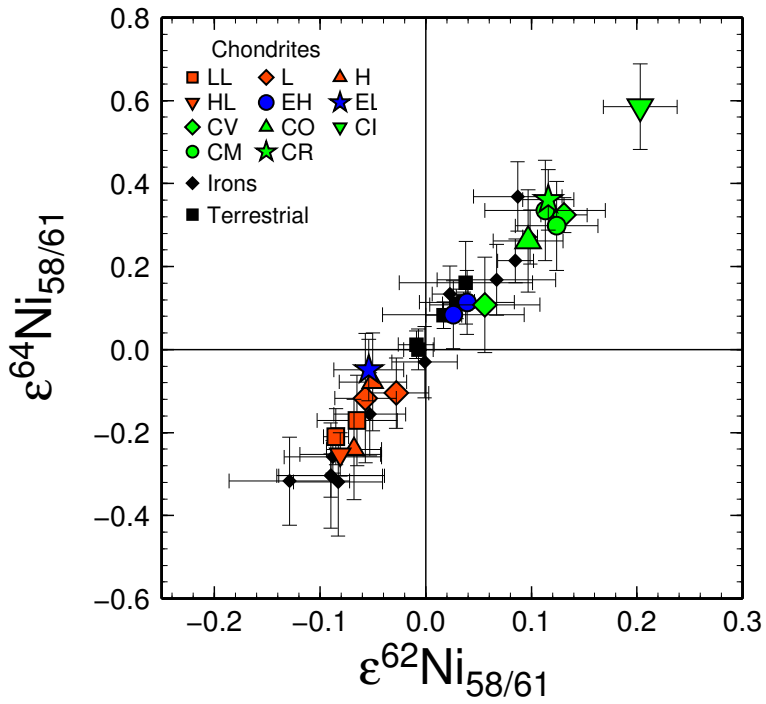

Fig. 1.— Figure showing the strong positive correlation between $\varepsilon^{64}\mathrm{Ni}_{\frac{58}{61}}$ and $\varepsilon^{62}\mathrm{Ni}_{\frac{58}{61}}$ for chondrites which has a slope of 3.003 ±0.166, see main text for regression details. Also shown are data for iron meteorites from Steele et al. (2011) which cover effectively the same range as the chondrites. Errors are 2 standard errors (2 s.e.). A colour version of this figure is available in the online edition.

The carbonaceous chondrites have the highest positive anomalies in $\varepsilon^{62}\mathrm{Ni}_{\frac{58}{61}}$ and $\varepsilon^{64}\mathrm{Ni}_{\frac{58}{61}}$, enstatite chondrites have approximately terrestrial ratios and the ordinary chondrites exhibit negative anomalies. This pattern is the same as that observed in other neutron-rich nuclides, e.g. $\varepsilon^{54}\mathrm{Cr}_{\frac{52}{50}}$ and $\varepsilon^{50}\mathrm{Ti}_{\frac{49}{47}}$ (e.g. Shukolyukov and Lugmair 2006; Trinquier et al. 2007; Trinquier et al. 2009) resulting in correlated anomalies, see Figure 2(b). Of the carbonaceous chondrites (CCs) Orgueil (CI) has the highest $\varepsilon^{62}\mathrm{Ni}_{\frac{58}{61}}$ and $\varepsilon^{64}\mathrm{Ni}_{\frac{58}{61}}$ ratios, which decrease through CV, CR, CM to CO. This order is consistent with that of $\varepsilon^{54}\mathrm{Cr}_{\frac{52}{50}}$ (Figure 2b) but opposite to $\varepsilon^{50}\mathrm{Ti}_{\frac{49}{47}}$ likely due to variable influence of CAIs on bulk Ti isotopic compositions (Trinquier et al. 2009). The iron meteorites reported by Steele et al. (2011) show essentially the same range in Ni isotopic compositions as the chondrites presented here. All carbonaceous, ordinary and EL enstatite chondrites are resolved from the terrestrial composition and only EH enstatite chondrites are indistinguishable

from the Earth in all mass-independent Ni isotope ratios. The latter are defined by analyses of natural terrestrial materials (e.g. the peridotites JP-1 and DTS-2) which yield $\varepsilon^{62}\mathrm{Ni}_{\frac{58}{61}}$ 0.036 ±0.010 and $\varepsilon^{64}\mathrm{Ni}_{\frac{58}{61}}$ 0.119 ±0.021 ‰, see Figure 1 (Steele et al. 2011). It should be noted that these samples differ slightly in their mass-independent Ni isotope ratios from the NIST SRM 986 reference. Steele et al. (2011) discuss this issue in detail and attribute this minor artefact to inaccuracies in the conventional approach of using a single exponential correction to account for instrumental and pre-analytical fractionation (see also Young et al. 2002). This should only significantly influence the moderately fractionated NIST SRM 986 composition but not those of our natural terrestrial or meteorite samples which only show minor variability in their mass-dependent Ni isotopic compositions, see Table 1 Steele et al. (2011) and Cameron et al. (2009).

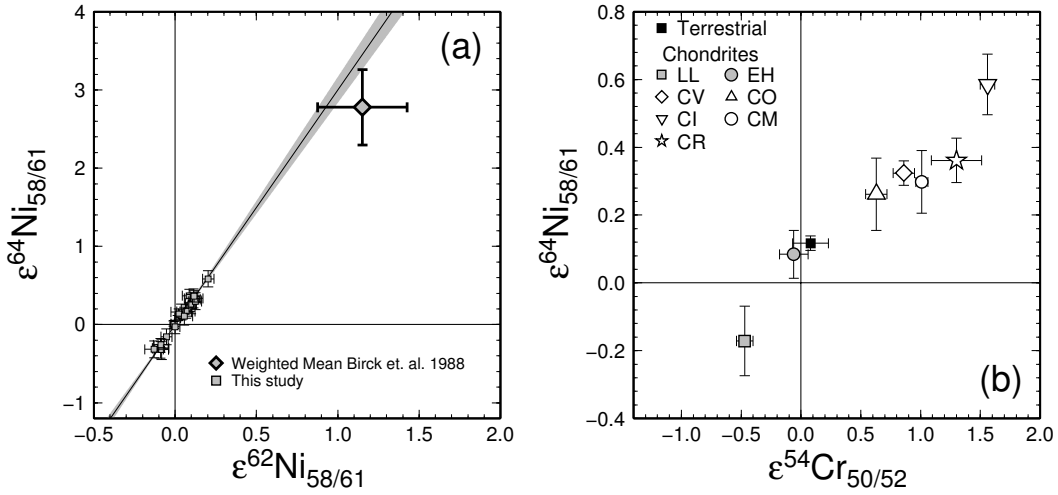

Fig. 2.— (a) Figure showing that the York regression through the data from Figure 1 (solid curve, 2 s.e. in grey) is within error of earlier CAI data from Birck and Lugmair (1988). The weighted mean of the Birck and Lugmair (1988) measurements with 2 s.e. error bars is also shown. (b) The correlation between $\varepsilon^{62}\mathrm{Ni}_{\frac{58}{61}}$ and $\varepsilon^{54}\mathrm{Cr}_{\frac{52}{50}}$ another neutron-rich iron group isotope thought to be produced in the same environment as ^{62}Ni and ^{64}Ni.

The relationship between $\varepsilon^{60}\mathrm{Ni}_{\frac{58}{61}}$ and either $\varepsilon^{62}\mathrm{Ni}_{\frac{58}{61}}$ (Figure 3) or $\varepsilon^{64}\mathrm{Ni}_{\frac{58}{61}}$ (not shown) is more complex and has been previously discussed by Regelous et al. (2008). Within the CCs there is a weak positive correlation between $\varepsilon^{60}\mathrm{Ni}_{\frac{58}{61}}$ and $\varepsilon^{62}\mathrm{Ni}_{\frac{58}{61}}$ that does not pass through terrestrial ratios, but is offset to positive $\varepsilon^{62}\mathrm{Ni}_{\frac{58}{61}}$ or negative $\varepsilon^{60}\mathrm{Ni}_{\frac{58}{61}}$. This trend is sequenced from high $\varepsilon^{60}\mathrm{Ni}_{\frac{58}{61}}$ and $\varepsilon^{62}\mathrm{Ni}_{\frac{58}{61}}$ in CI, through CO, CM, CV to CR, which is different to the order of these groups

in the $\varepsilon^{64}Ni_{\frac{58}{61}}$ vs. $\varepsilon^{62}Ni_{\frac{58}{61}}$ array. The ordinary chondrite (OC)s have negative $\varepsilon^{60}Ni_{\frac{58}{61}}$ and, again, EH enstatite chondrites (ECs) have terrestrial ratios. Iron meteorites again span a similar range of $\varepsilon^{60}Ni_{\frac{58}{61}}$ as the chondrites and only one iron meteorite sample, the IC iron meteorite Bendegó, is not resolved from terrestrial ratios (Steele et al. 2011).

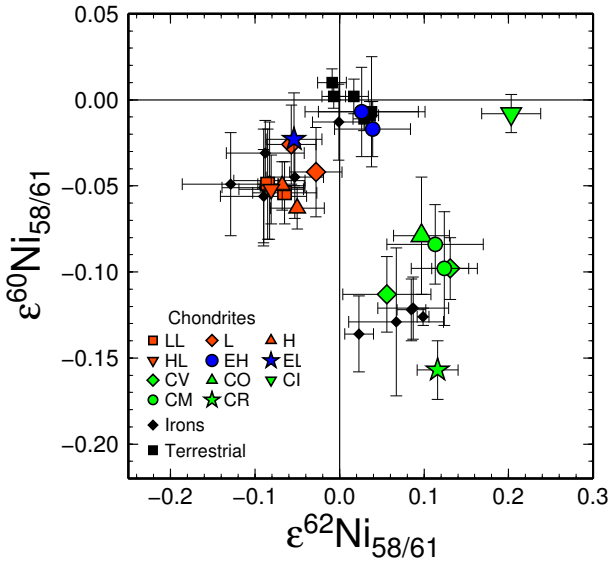

Fig. 3.— Plot showing $\varepsilon^{60}Ni_{\frac{58}{61}}$ vs. $\varepsilon^{62}Ni_{\frac{58}{61}}$. These data are consistent with the data of Regelous et al. (2008) but at slightly higher precision. No overall correlation exists as discussed previously by Regelous et al. (2008). A colour version of this figure is available in the online edition.

2.1. Location of anomalies

The slope of the meteorite array in $\varepsilon^{64}Ni_{\frac{58}{61}}$ vs. $\varepsilon^{62}Ni_{\frac{58}{61}}$ (3.003 ±0.166) is within error of the slope 2.96 predicted if anomalies were produced by variability in ^{58}Ni alone. This observation is worthy of investigation because variable ^{58}Ni anomalies are a simpler explanation than correlated variations on ^{62}Ni and ^{64}Ni. We note that variability on ^{58}Ni could be caused by interferences on this isotope during analysis, but we have extensively discussed and eliminated this possibility in a previous contribution (Steele et al. 2011).

To test the hypothesis that there are anomalies on ^{58}Ni we have determined to high precision the 'absolute ratios' of two chondrites, CI CC Orgueil and the H-type

	$\varepsilon^{58/61}$Ni	2 s.e.	$\varepsilon^{60/61}$Ni	2 s.e.	$\varepsilon^{61/61}$Ni	2 s.e.	$\varepsilon^{62/61}$Ni	2 s.e.	$\varepsilon^{64/61}$Ni	2 s.e.
Butsura	-3.00	0.22	-1.03	0.07	0.00	0.00	0.91	0.09	2.69	0.23
Orgueil	-2.17	0.25	-0.72	0.08	0.00	0.00	0.90	0.09	2.65	0.26

Table 2: Table showing high precision absolute ratio data for Orgueil (CI) and Butsura (OC). Errors quoted include all sources of uncertainty discussed above, see section A.3.2

OC Butsura, which span the range of $\varepsilon^{62}\text{Ni}_{\frac{58}{61}}$ and $\varepsilon^{64}\text{Ni}_{\frac{58}{61}}$ anomalies. This has been achieved by coupling mass-independent measurements with high precision mass-dependent data determined by double spiking (see appendix), using a technique developed from Cameron et al. (2009). These results are shown in Table 2 and Figure 4 as parts per ten thousand (‱) difference of each isotope normalised to ^{61}Ni and NIST SRM 986. As is evident in Figure 4 the dominant character of the two samples is a general positive slope, indicating significant mass fractionation between the samples and the reference standard NIST SRM 986 (see, Steele et al. 2011). Deviations from the dashed line, however, reflect the more subtle mass-independent anomalies.

Whilst the ^{62}Ni/^{61}Ni and ^{64}Ni/^{61}Ni ratios are identical within error in these two meteorites, differences in ^{58}Ni/^{61}Ni are well resolved. The absolute ratios also show that a small anomaly remains on ^{60}Ni. These data are strong evidence that the anomalies in internally normalised Ni isotope ratios are in fact due to anomalies on the neutron-poor isotope ^{58}Ni (and ^{60}Ni) and not the neutron-rich isotopes ^{64}Ni and ^{62}Ni.

2.2. Normalisation

Given our new inference that the anomalies in Ni reside on ^{58}Ni we further present our data normalised to ^{62}Ni/^{61}Ni in Figures 5(a) and (b). Using this normalisation there is broadly correlated variation between $\varepsilon^{58}\text{Ni}_{\frac{62}{61}}$ and $\varepsilon^{60}\text{Ni}_{\frac{62}{61}}$, but there is still a small offset between the arrays of the CCs and OCs, EC and terrestrial samples, respectively. As expected there is very little variation in $\varepsilon^{64}\text{Ni}_{\frac{62}{61}}$, with almost all data being within error of zero. We note that the slope of the data in $\varepsilon^{60}\text{Ni}_{\frac{62}{61}}$ vs. $\varepsilon^{58}\text{Ni}_{\frac{62}{61}}$ space is approximately one half. This slope could result from a variable interference on mass 61 but this possibility can be ruled out because the required associated anti-correlation in $\varepsilon^{60}\text{Ni}_{\frac{62}{61}}$ vs. $\varepsilon^{64}\text{Ni}_{\frac{62}{61}}$ is not present

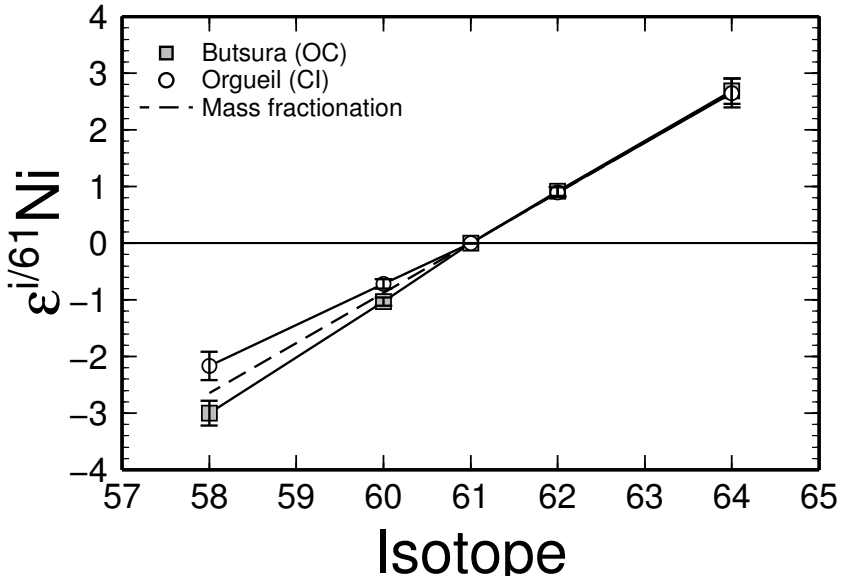

Fig. 4.— Figure showing absolute Ni isotope ratios, ^{i}Ni/^{61}Ni, for Orgueil and Butsura in parts per ten thousand (‱) difference from NIST SRM 986. These data show strong evidence that Ni isotope heterogeneity is located on ^{58}Ni and ^{60}Ni and not on ^{62}Ni and ^{64}Ni.

(not shown). We have also discussed in more detail elsewhere (Steele et al. 2011) the reasons we discount the possible presence of this type of interference in our analyses.

It is clearly useful to examine the data re-normalised to ^{62}Ni/^{61}Ni, as presented in Figure 5 in order to most readily visualise the isotopic variations, but this may not necessarily be the most effective way of quantitatively analysing our data. The ^{62}Ni/^{61}Ni normalisation uses two minor isotopes with only one mass unit separation which results in large propagated errors in the final mass-independent data. Therefore, in the rest of this study we continue to use the ^{58}Ni/^{61}Ni ratio for normalisation, which results in higher precision data. Moreover, existing work on mass-independent Ni isotope variations has already presented data normalised to two different ratios and a third, new, normalisation would only add confusion. Whilst it might initially seem obtuse to employ a scheme that uses a normalising isotope ratio known to be strongly perturbed by nucleosynthetic effects, we emphasis that added nucleosynthetic components will likely influence all isotopes, albeit to different degrees. As long as potential anomalous contributions from all isotopes are considered in subsequent treatments no problems will arise from the

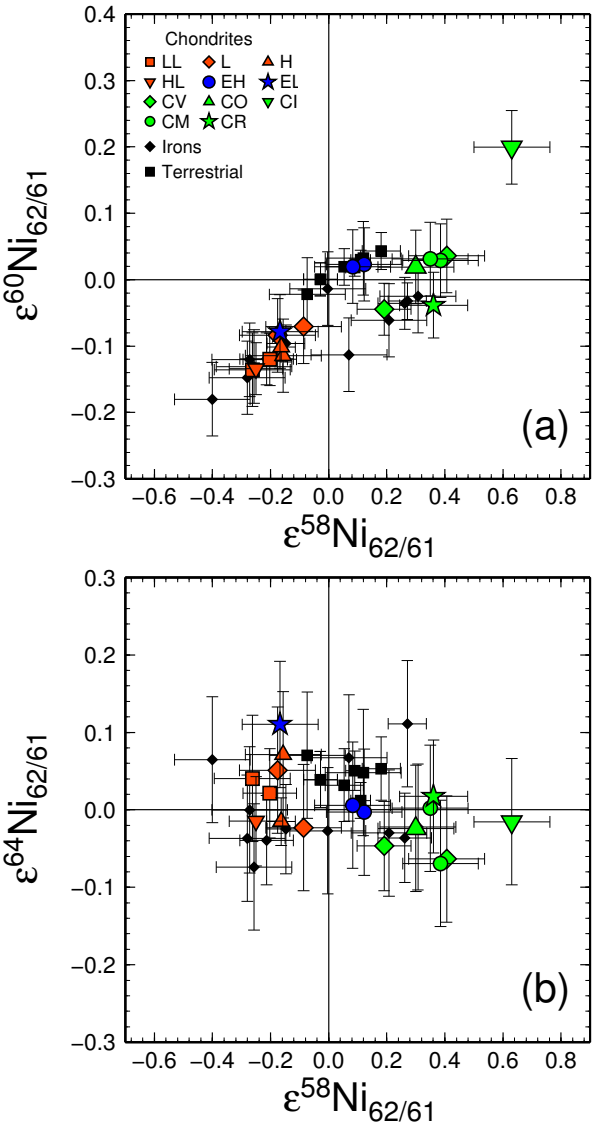

Fig. 5.— Plots showing the same data as presented in Figure 1 and Table 1 re-normalised to $^{62}Ni/^{61}Ni$. Colour versions of these figures are available in the online edition.

manner in which the data are reported.

3. Discussion

3.1. Stellar origin of nucleosynthetic heterogeneity

Given previous measurements of CAIs (Birck and Lugmair 1988) lie on an extension of the Ni isotopic array defined by our bulk meteorite analyses, see Figure 2(a), variable proportions of a single anomalous component can potentially explain the Solar System heterogeneity evident in $\varepsilon^{64}\mathrm{Ni}_{\frac{58}{61}}$ vs. $\varepsilon^{62}\mathrm{Ni}_{\frac{58}{61}}$ plots. Since mass-independent anomalies in Ni are not thought to be generated within the Solar System, the observed heterogeneity in compositions is likely the result of incomplete mixing, or 'unmixing' of a common carrier phase. It is intriguing that the volatile rich CI meteorites, that likely accreted beyond the snow line, are closer in composition to the highly refractory CAIs, thought to be formed closer to the sun than the other more volatile-poor bulk meteorites (e.g. OCs) that presumably represent material from intermediate nebula radii. The more prosaic explanation that the bulk meteorite Ni isotopic variability simply reflects variable proportions of CAIs in different meteorite groups is implausible since CAIs are neither a volumetrically dominant component of most chondrites, nor a dominant repository of Ni. Moreover, no CAIs are found in the CI CC Orgueil, the bulk meteorite which has the closest isotopic composition to CAIs. Similar observations and inferences have been made for the isotope systematics of other iron group elements, e.g. Ti and Cr (Trinquier et al. 2009).

An initial objective is thus to identify the stellar origin of the component which occurs in different proportions within different meteorite types. We subsequently address the processes by which this material can be variably distributed across the Solar System.

The elements of the iron abundance peak are dominantly produced in stars by nuclear statistical equilibrium, the e-process (Burbidge et al. 1957). The e-process is thought to occur in a range of stellar sources and these different nucleosynthetic environments can produce very large and contrasting isotope anomalies. Such nucleosynthetic components have isotopic anomalies many orders of magnitude larger than the total variation in the Solar System. In order to assess the influence of adding such exotic material to mass-independent isotope ratios in the Solar System, the contribution to all isotopes needs to be considered. Below such a treatment is presented, which allows us to identify plausible nucleosynthetic components that can generate correlated variability in mass-independent isotopic

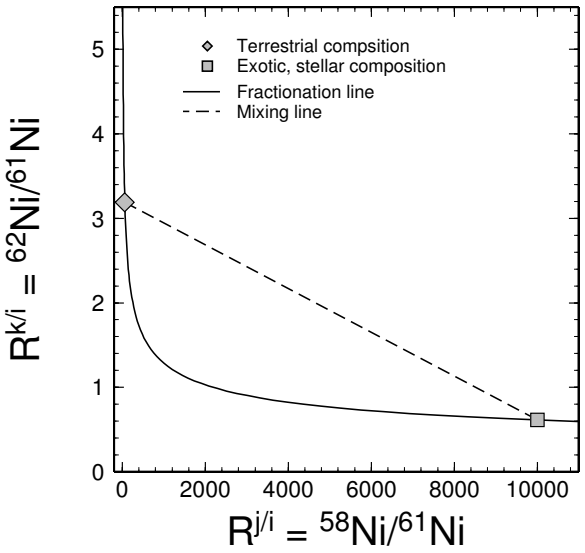

Fig. 6.— Plot showing the difference between the path of exponential fractionation and mixing in three isotope space at extreme ratios.

ratios in Solar System materials, such as shown in Figure 1.

A key aspect in our approach is accounting for nucleosynthetic perturbations of the normalising isotope ratio. Solar System samples are corrected for natural and instrumental fractionation using the exponential law (Russell et al. 1978),

$$R^{j/i}_{\rm frac} = R^{j/i}_{\rm ref} \left(\frac{m_j}{m_i} \right)^{\beta} \tag{1}$$

where β is the exponential fractionation factor, $R^{j/i}_{\rm ref}$ and $R^{j/i}_{\rm frac}$ are the ratios of isotope j to isotope i in a reference material and a sample fractionated from that reference material. Two ratios, fractionated mass-dependently, e.g. $R^{k/i}$ and $R^{j/i}$, form an exponential relationship shown in Figure 6. If this passes through the bulk terrestrial composition, it is the terrestrial fractionation line (TFL). If we take $R^{j/i}_{\rm ref}$ as our normalising ratio, a positive internally normalised mass-independent anomaly in $R^{k/i}$ is defined as deviation above the exponential law at constant $R^{j/i}_{\rm ref}$, and when presented as parts per ten thousand difference to a terrestrial standard is written $\varepsilon^k R_{j/i}$.

In Fig 6 we show an isotopically extreme, stellar component (square) which we have placed on the TFL for illustrative purposes. Positive mass-independent

anomalies can be created by mixing this exotic stellar component with a terrestrial composition (diamond), since in this plot, where the two axes are ratios with common denominators, mixing defines a straight line and so always lies above the mass fractionation curve in this illustration. If we had erroneously normalised the composition of the exotic component to a terrestrial ^{58}Ni/^{61}Ni before calculating the effects of mixing, no anomaly would be apparent. The effects of mixing between solar and exotic compositions can be calculated for each isotope of interest and the resulting mixture suitably normalised to the conventional solar reference value, as discussed by Simon et al. (2009). However, we illustrate below, that for a small amount of added material, the co-variation of two mass-independent isotope ratios of a given element can be calculated more readily.

At very small degrees of fractionation the exponential law approximates to a straight line with a slope of $\ln(m_k/m_i)/\ln(m_j/m_i)$ as illustrated by the solid line in Figure 7(a). In this figure the x-axis is the normalising ratio, $\varepsilon^{58/61}$Ni, and the y-axis is the ratio to be normalised, $\varepsilon^{62/61}$Ni. Hence, the mass-independent ratio of a composition in this 3-isotope space is equal to the vertical distance measured from the solid line. The dashed line in Figures 7(a) is the mixing line to a highly exotic nucleosynthetic composition at the point ($\varepsilon^{j/i}_{\rm nuc}R$, $\varepsilon^{k/i}_{\rm nuc}R$). The difference in slopes of these lines is given by,

$$\Delta s^{k/i}_{j/i} = s_{\rm mix} - s_{\rm frac} = \left(\frac{\varepsilon^{k/i}_{\rm nuc}R}{\varepsilon^{j/i}_{\rm nuc}R}\right) - \left(\frac{\ln(m_k/m_i)}{\ln(m_j/m_i)}\right), \qquad (2)$$

where $\varepsilon^{k/i}_{\rm nuc}R$ and $\varepsilon^{j/i}_{\rm nuc}R$ are the compositions of a modelled nucleosynthetic environment. The second term on the right hand side is the slope of fractionation by the exponential law, see Young et al. (2002). Figure 7(b) has k (= ^{62}Ni) replaced by l (= ^{64}Ni) but is otherwise identical to Figure 7(a). The corresponding expression for the difference in slopes, $\Delta s^{l/i}_{j/i}$, is similar to equation 2.

If a small fraction of the exotic component is mixed into a nebula (with composition $\varepsilon = 0$) then the resulting composition of the mixture can be written $\varepsilon^{x/i}_{\rm nuc}R \cdot f$, where f is the mixing parameter and x is j, k or l. The resulting mass-independent isotope ratios of the mixture can be written in terms of the difference in the slopes thus,

$$\varepsilon^{k}R_{j/i} = \Delta s^{k/i}_{j/i}(\varepsilon^{j/i}_{\rm nuc}R \cdot f) \qquad (3)$$

and

$$\varepsilon^{l}R_{j/i} = \Delta s^{l/i}_{j/i}(\varepsilon^{j/i}_{\rm nuc}R \cdot f). \quad (4)$$

Dividing equation 4 by equation 3 yields,

$$\varepsilon^{l}R_{j/i} = \frac{\Delta s^{l/i}_{j/i}}{\Delta s^{k/i}_{j/i}} \cdot \varepsilon^{k}R_{j/i}. \quad (5)$$

Hence, in a plot of $\varepsilon^{l}R_{j/i}$ vs. $\varepsilon^{k}R_{j/i}$ mixtures will lie on a straight line with slope $\Delta s^{l/i}_{j/i}/\Delta s^{k/i}_{j/i}$.

Thus for a system of four, or more, isotopes the slope produced on a plot of two mass-independent isotope ratios can be calculated for the admixture of a small amount of exotic material to the Solar System.

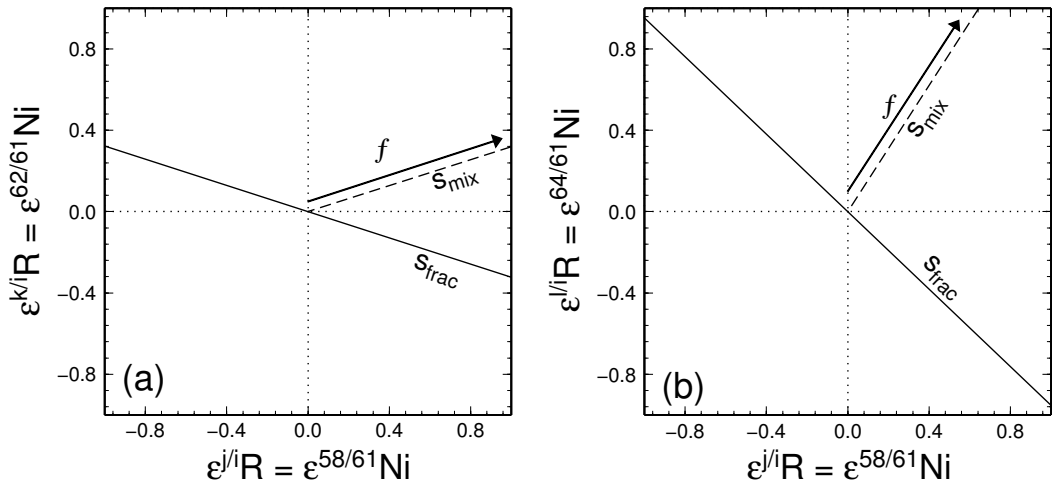

Fig. 7.— Schematic plots showing the difference between the path of exponential fractionation and mixing on three isotope plots. $s_{\rm frac}$ is the path of exponential fractionation given by the slope $\ln(m_x/m_i)/\ln(m_j/m_i)$ where x can be k or l, $s_{\rm mix}$ is the path of mixing between the average Solar System composition and the an anomalous nucleosynthetic composition, and f is the fraction of the distance along the mixing line from the origin to the anomalous end-member.

In the case of Ni, k and l, may be any isotope of interest, for example ^{64}Ni and ^{62}Ni, while j and i are once again the normalising isotopes ^{58}Ni and ^{61}Ni. The ratio of the slopes, $\Delta s^{64/61}_{58/61}/\Delta s^{62/61}_{58/61}$, gives the slope of mixing between a terrestrial composition and an exotic component in relative normalised isotope space, e.g. $\varepsilon^{64}{\rm Ni}_{\frac{58}{61}}$ vs. $\varepsilon^{62}{\rm Ni}_{\frac{58}{61}}$. The slopes obtained for different astrophysical environments

259 can then be compared with the slope defined by anomalies in bulk meteorites. By
260 finding slopes from nucleosynthetic environments that match those in the Solar
261 System array, it may be possible to identify the particular nucleosynthetic envi-
262 ronment that created the component responsible for the Ni isotope variations in
263 bulk meteorites. It must be stressed that it doesn't matter on which isotopes the
264 anomalies reside, e.g. on ^{58}Ni or ^{62}Ni and ^{64}Ni because this method includes all
265 contributions from the normalising and reported ratios.

266 In order to calculate such a slope for an element, two co-varying internally nor-
267 malised ratios are required. This means at least three independent isotope ratios,
268 i.e. four isotopes. Of existing data in the literature and this study, for Fe group
269 transition elements only Ti and Ni satisfy these conditions. Chromium has enough
270 isotopes, but because of the decay of the abundant but variably distributed ^{53}Mn,
271 initial values of ^{53}Cr are potentially masked by different radiogenic contributions.
272 Due to chemical fractionation during transport from stellar sources or early Solar
273 System processing, inter-element slopes are unlikely to show original correlations.
274 Since Ni is the primary objective of this study, fitting the Ni isotopes is our major
275 criterion. However, the slope of the Solar System array in Ti isotope space is also
276 considered.

277 ### *3.1.1. Application to Ni isotopes*

278 The isotopic composition of different bulk nucleosynthetic environments has
279 been modelled by many studies. For SN Ia we have used data from Woosley
280 (1997); Travaglio et al. (2004); Iwamoto et al. (1999); Hashimoto (1995); Maeda
281 et al. (2010). For SN II we have used data from Iwamoto et al. (1999); Umeda and
282 Nomoto (2002); Nomoto et al. (1997); Rauscher et al. (2002); Hashimoto (1995).
283 We have used AGB models kindly provided by Davis (pers. comm. 2009). The
284 composition of material given off by Wolf Rayet stars has been estimated using
285 the wind from high mass (>35 $M_\odot$) supernova models of Rauscher et al. (2002).
286 In Figure 8(a) we show the slopes that would be produced in $\varepsilon^{64}\mathrm{Ni}_{\frac{58}{61}}$ vs. $\varepsilon^{62}\mathrm{Ni}_{\frac{58}{61}}$
287 by mixing the bulk ejecta from the sources modelled in the studies above with
288 typical Solar System material. For reference these slopes are plotted against the
289 ^{58}Ni/^{61}Ni of the bulk ejecta to indicate further the wide range of compositions
290 produced in different stellar environments. The model slopes can be compared to
291 that observed in Solar System materials in Figure 1, shown as a dashed line in

Figure 8(a). The mass-independent Ni isotopic variability seen in the Solar System can thus be accounted for by addition to the solar nebula of material derived from model sources that plot within the dotted lines of Figure 8(a). It is clear that in $\varepsilon^{64}\mathrm{Ni}_{\frac{58}{61}}$ vs. $\varepsilon^{62}\mathrm{Ni}_{\frac{58}{61}}$ space, the majority of the nucleosynthetic environments (shown in Figure 8(a)) do not produce appropriate model slopes. There is one SN Ia model (C-DDT/def of Maeda et al. 2010) that could mix with the solar nebula to produce a slope within error of that observed in Solar System materials. In addition, one SN II model (S25 of Rauscher et al. 2002) differs by only 2.05 σ from the slope observed in meteorites and is the only other model within 3 σ so we shall include it in the discussion. Mixing of material from the two models of AGB stars and the estimates of the composition of material lost from Wolf Rayet stars does not produce an appropriate slope within error of Solar System materials.

As is shown above (section 2.2), the anomalies in Ni isotopes likely reside on ^{58}Ni. Since our treatment of the modelled supernova compositions includes effects on all isotopes, those which match the slope in $\varepsilon^{64}\mathrm{Ni}_{\frac{58}{61}}$ vs. $\varepsilon^{62}\mathrm{Ni}_{\frac{58}{61}}$ may do so either because ^{62}Ni and ^{64}Ni happen to be produced and mixed in with the correct abundances, or because the dominant isotope is ^{58}Ni. Therefore, we need to examine further the potentially successful solutions in Figure 8(a) to see if they are a result of the requisite ^{58}Ni enrichment. The results are shown in Fig 8(b) where the absolute Ni isotope ratios of the two models show that only the SN Ia model matches the slope by sole overproduction of ^{58}Ni. Since SN Ia nucleosynthesis is typically highly neutron enriched, however, the majority of SN Ia models do not match the meteorites slope. The only SN II model that matches the slope in $\varepsilon^{64}\mathrm{Ni}_{\frac{58}{61}}$ vs. $\varepsilon^{62}\mathrm{Ni}_{\frac{58}{61}}$ does not have a ^{58}Ni anomaly; it matches the slope by chance overproduction of ^{62}Ni and ^{64}Ni in the correct proportions. Therefore, this SN II model cannot provide the observed Ni isotope heterogeneity to the Solar System.

A further requirement for a plausible source of Ni isotope heterogeneity is that the same environment should be capable of producing other transition element isotope heterogeneity. One such element whose isotopic composition has recently been investigated in bulk samples by several studies is Ti (Leya et al. 2008, 2009; Trinquier et al. 2009). Like Ni, Ti exhibits a strong intra-element isotopic correlation between $\varepsilon^{50}\mathrm{Ti}_{\frac{49}{47}}$ and $\varepsilon^{46}\mathrm{Ti}_{\frac{49}{47}}$, while showing no variation in $\varepsilon^{48}\mathrm{Ti}_{\frac{49}{47}}$ (Trinquier et al. 2009). Titanium isotope anomalies also correlate with Ni isotope anomalies suggesting they may share a common source. Therefore, for the SN Ia model which produces an appropriate Ni component to account for Solar System variability should similarly generate Ti of the correct isotopic composition

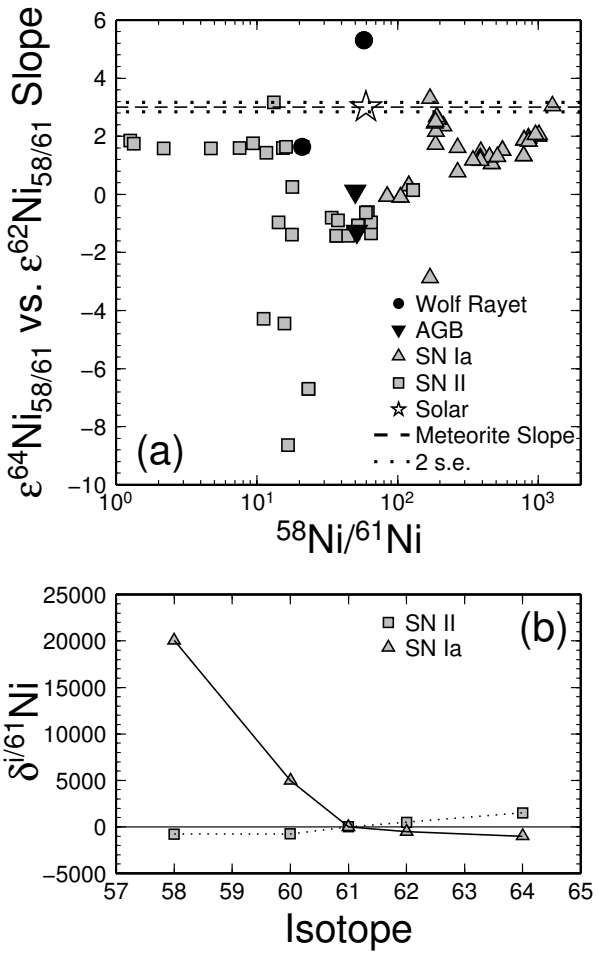

Fig. 8.— (a) Figure showing the slope in $\varepsilon^{64}\mathrm{Ni}_{\frac{58}{61}}$ vs. $\varepsilon^{62}\mathrm{Ni}_{\frac{58}{61}}$ space that results from mixing exotic material from various astrophysical environments with typical Solar System material. Models assume that all short lived nuclides have decayed. Data from Woosley (1997); Travaglio et al. (2004); Iwamoto et al. (1999); Hashimoto (1995); Maeda et al. (2010) for SN Ia, Iwamoto et al. (1999); Umeda and Nomoto (2002); Nomoto et al. (1997); Rauscher et al. (2002); Hashimoto (1995) for SN II, Davis (pers. comm. 2009) for AGB. The composition of material lost from Wolf Rayet stars has been estimated using the wind from high mass (>35 $M_\odot$) supernova models of Rauscher et al. (2002). The dashed line indicates the slope observed in Solar System materials, Figure 1, with 2 s.e. error (dotted lines). (b) Figure showing the absolute ratios for the models (SN Ia (C-DDT/def of Maeda et al. 2010) and SN II model (S25 of Rauscher et al. 2002)) which match the slope in observed in Solar System materials.

to account for the slopes of the meteorite arrays in Ti isotope space.

The slope observed in Solar System samples by Trinquier et al. (2009) between $\varepsilon^{50}\mathrm{Ti}_{\frac{49}{47}}$ and $\varepsilon^{46}\mathrm{Ti}_{\frac{49}{47}}$ is 5.48 ±0.27, while the slopes for both $\varepsilon^{50}\mathrm{Ti}_{\frac{49}{47}}$ vs. $\varepsilon^{48}\mathrm{Ti}_{\frac{49}{47}}$ and

$\varepsilon^{46}Ti_{\frac{49}{47}}$ vs. $\varepsilon^{48}Ti_{\frac{49}{47}}$ are zero. The supernova model that matches the Ni isotope constraints generates slopes in Ti of $\varepsilon^{50}Ti_{\frac{49}{47}}$ vs. $\varepsilon^{46}Ti_{\frac{49}{47}}$= -2.33, $\varepsilon^{50}Ti_{\frac{49}{47}}$ vs. $\varepsilon^{48}Ti_{\frac{49}{47}}$ = -3.9 and $\varepsilon^{46}Ti_{\frac{49}{47}}$ vs. $\varepsilon^{48}Ti_{\frac{49}{47}}$ = 0.6. These clearly do not match the those observed in meteorites and so cannot provide any supporting evidence that bulk ejecta from this unique SN Ia model can account for iron group isotopic variability in the Solar System.

In summary, addition of bulk ejecta from an SN II cannot account for the Ni isotope heterogeneity to the Solar System, whilst only a single SN Ia model can account for both the correct slope of meteoritic material in $\varepsilon^{62}Ni_{\frac{58}{61}}$, $\varepsilon^{64}Ni_{\frac{58}{61}}$ space by providing ^{58}Ni anomalies. However, one model is not a strong case for the source of Ni isotope heterogeneity. Moreover, this model cannot account for the heterogeneity in Ti isotopes observed by Trinquier et al. (2009) so cannot account for Fe-group isotope heterogeneity in general. Therefore, no calculated bulk supernova inputs seem appropriate to explain Solar System variation so we further examine the compositions of individual nucleosynthetic shells within supernovae.

3.1.2. Supernova components

Type Ia supernovae have three distinct components: a large ^{56}Ni core, a region of Fe abundance peak elements and an outer region of lighter intermediate mass elements up to Ca (Kasen et al. 2009). Dynamical models of SN Ia explosions show that the inner regions consisting of the ^{56}Ni core and Fe group elements undergo Rayleigh-Taylor instabilities and are likely to be turbulently mixed (Kasen et al. 2009). This may suggest that bulk SN Ia are likely to give homogenised isotope ratios for iron group elements and that treatment beyond what we attempted in the last section in not warranted.

Conversely, SN II are explosions of much more massive stars 3-70 $M_\odot$ so effective homogenisation is less likely. Type II supernovae are normally split into eight zones named after the two most abundant elements (Meyer et al. 1995). Thus, we consider the isotope anomalies found from individual shells of SN II as in several recent studies (e.g. Dauphas et al. 2008; Moynier et al. 2009; Liu et al. 2009) and in established work on discrete pre-solar grains (e.g. Zinner 2003).

Rauscher et al. (2002) computed isotopic abundances for multiple spherical shells within an SN II for different events over a range of pre-supernova masses (15

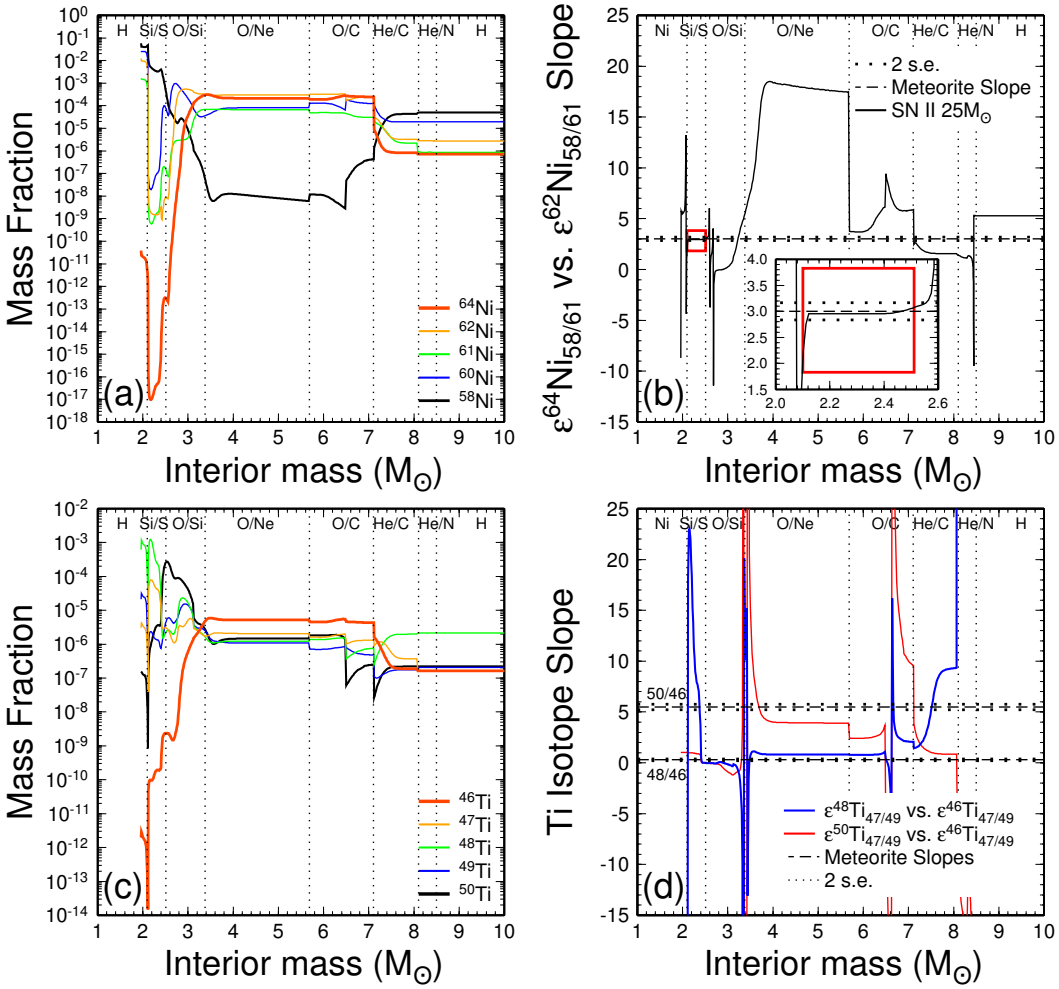

Fig. 9.— (a) Diagram showing the zonal yields of Ni isotopes from a 25 $M_\odot$ supernova from Rauscher et al. (2002). (b) The slope produced in $\varepsilon^{64}Ni_{\frac{58}{61}}$ vs. $\varepsilon^{62}Ni_{\frac{58}{61}}$ space by incomplete mixing of small amounts of these zones into the Solar System, inset is an expanded view of the Si/S zone. See text for details. (c) The zonal yields of Ti isotopes through a 25 $M_\odot$ supernova also from Rauscher et al. (2002). (d) The slope produced in $\varepsilon^{46}Ti_{\frac{49}{47}}$ vs. $\varepsilon^{50}Ti_{\frac{49}{47}}$ $\varepsilon^{48}Ti_{\frac{49}{47}}$ vs. $\varepsilon^{46}Ti_{\frac{49}{47}}$ and $\varepsilon^{48}Ti_{\frac{49}{47}}$ vs. $\varepsilon^{50}Ti_{\frac{49}{47}}$ isotope space. Also shown in both diagrams are the names of the zones given by the two most abundant elements, after Meyer et al. (1995). These diagrams show that mixing incompletely material from the Si/S zone into the early Solar System would produce the slope observed in Ni isotopes in the bulk meteorite materials. Though shown for the 25 $M_\odot$ supernova only, this is true of all the Rauscher et al. (2002) supernova models. Colour versions of these figures are available in the online edition.

363 - 40 $M_\odot$), see http:/nucastro.org. These shells can be treated in the same way as
364 the bulk supernova models discussed previously and the slope in mass-independent

isotope space can be determined for variable mixing of a small amount of each shell into the Solar System. For the same reason as discussed in Meyer et al. (1995), namely a balance between galactic occurrence and mass ejected, we examine in detail a 25 $M_\odot$ supernova model. Other supernova masses have been examined and are referred to where relevant.

The production of Ni isotopes through a 25 $M_\odot$ SN II is shown in 9(a), and the slopes produced by mixing this material in to the Solar System in 9(b). These figures illustrate that the addition of material from the Si/S zone of a SN II would produce the same slope in $\varepsilon^{64}\mathrm{Ni}_{\frac{58}{61}}$ vs. $\varepsilon^{62}\mathrm{Ni}_{\frac{58}{61}}$ space as observed in the meteorite sample array. Whilst only shown for a 25 $M_\odot$ SN II, it is interesting to note that the same is true for all other stellar masses, 15 $M_\odot$, 19 $M_\odot$, 20 $M_\odot$, 30 $M_\odot$, 35 $M_\odot$ and 40 $M_\odot$, modelled by Rauscher et al. (2002). Moreover, as seen in Figure 9(a), the Si/S zone also produces ^{58}Ni as the dominant Ni isotope - 5 orders of magnitude higher than the next most abundant Ni isotope. Therefore, the Si/S zone meets all the criteria as the source of Ni isotope heterogeneity in the early Solar System. In addition to the models of Rauscher et al. (2002) the compositions of different zones of a 25 $M_\odot$ SN II were computed by Meyer et al. (1995). The results of this independent model also show large overproduction of ^{58}Ni in the Si/S zone and produce the correct slope in $\varepsilon^{64}\mathrm{Ni}_{\frac{58}{61}}$ vs. $\varepsilon^{62}\mathrm{Ni}_{\frac{58}{61}}$ (2.97) within error of the slope of Solar System material. The work of Meyer et al. (1995), therefore, provides supporting evidence that overproduction of ^{58}Ni in the Si/S zone is a general feature of SN II making a robust case for SN II being the source of Ni isotope heterogeneity in the Solar System.

The corresponding Ti isotope compositions of SN II shells and the slopes generated in mass-independent isotope plots as a result of mixing this material with the Solar System are shown in Figures 9(c) and (d), respectively. The measurements of Trinquier et al. (2009) define a slope in $\varepsilon^{50}\mathrm{Ti}_{\frac{49}{47}}$ vs. $\varepsilon^{46}\mathrm{Ti}_{\frac{49}{47}}$ space of 5.48 $\pm$0.27 and slopes of zero in $\varepsilon^{48}\mathrm{Ti}_{\frac{49}{47}}$ vs. $\varepsilon^{46}\mathrm{Ti}_{\frac{49}{47}}$ and $\varepsilon^{48}\mathrm{Ti}_{\frac{49}{47}}$ vs. $\varepsilon^{50}\mathrm{Ti}_{\frac{49}{47}}$. As can be seen from Figure 9(d) none of the individual zones match precisely the slopes observed in all three systems for Solar System material. However, the upper section of O/Ne zone is very close. This is an interesting finding, as from a qualitative consideration of the very different settings for dominant ^{46}Ti and ^{50}Ti production Trinquier et al. (2009) inferred that the correlated Solar System anomalies must result from the contributions of several stellar components. This study did not consider the potential effects on normalising isotopes, nor did a subsequent discussion by Leya et al. (2009). Therefore the observation that a single source could

account for all Ti isotopic variability recorded in meteorites is a notable result.

As discussed above the more anomalies a nucleosynthetic environment can explain the more robust the case for it providing the source of isotope heterogeneity in the early Solar System. Therefore it is significant that a single SN II can provide the Ni and Ti anomalies observed in the Solar System. However, it cannot be ignored that the Ti isotope anomalies that match Solar System materials are not found in the same zones as those that produce appropriate Ni isotope compositions. On face value this implies that the SN II is an unlikely source of Solar System isotope heterogeneity, but it may be possible to decouple isotope anomalies of different elements. For example, different shells may produce condensates with dramatically different chemical or physical properties. Thus, processing during transport in the interstellar medium or within the Solar System may generate isotopic anomalies by differential processing of pre-solar grains with radically different isotopic compositions. We consider scenarios in more detail in section 3.3.

3.1.3. Combinations of supernova shells

Previous studies have often considered 'mass-cuts' of a supernova (see Rauscher et al. 2002, for a discussion of mass-cut location in these models); the averaged composition of material beyond a critical radius that is believed to be ejected rather than collapse onto the remnant core. We can also calculate the Ni isotope compositions of SN II ejecta for various mass-cuts to investigate if the Ni isotope anomalies observed in the Solar System can be provided by a single mass-cut. The results of this are shown in Figures 10(a) and (b), which show that a single mass-cut cannot provide the correct slope or the ^{58}Ni anomaly.

An important finding from pre-solar grains, believed to be delivered from supernovae (the so-called X-grains), is that their compositions reflect contributions of different elements from different zones of SN II events (e.g. Zinner 1998, 2003; Hammer et al. 2010). For example, Zinner (1998, 2003) suggested that presolar silicon carbide X-grains found in meteorites required input from the Ni and Si/S zones, to account for large excesses of ^{28}Si and ^{44}Ca together with material from the He/C zone to provide the carbon. Hoppe et al. (2010) suggested that molecule formation before mixing and grain formation can help account for the intimate association of such contrasting isotopic signatures. Recent work by Marhas et al. (2008) documents the Ni and Fe isotope compositions of X-grains and infers they

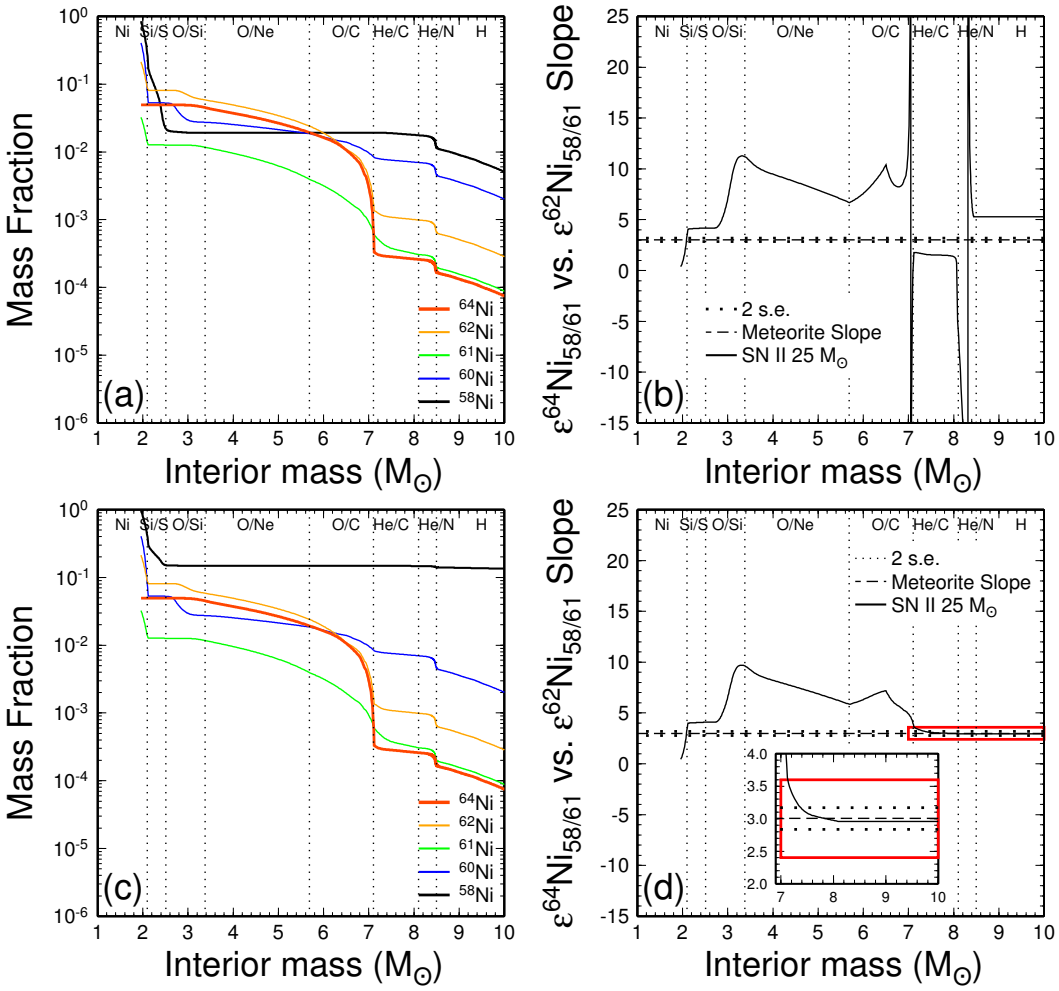

Fig. 10.— (a) and (b) show the integrated shell yields from the outside of the supernova inwards and the slope produced by mixing of these shells into the Solar System. They show that neither the ^{58}Ni anomaly nor the correct slope are produced by these integrated compositions. (c) and (d) show the same as (a) as (b) but in addition, mixing of the homogenised composition for the Si/S zone in to the integrated composition. They show that the Ni isotope signatures of the outer zones of the supernova (H, He/N, He/C) may be dominated by that of the ^{58}Ni from the Si/S zone, while those of the middle zones (O/Si, O/Ne, O/C) are not. Colour versions of these figures are available in the online edition.

are most compatible with nucleosynthesis in the He/N and He/C zones, which again contrasts with the ^{28}Si excesses of the SiC hosts. These observation show that specific phases can carry distinctive isotopic signatures from different parts of a supernova. Although the SiC X-grains identified are not themselves an appropriate component to account for the Solar System variability of Ni, other phases may

specifically sample Ni from a zone that does fulfil the isotopic requirements.

The suggestion that anomalies observed in meteorites may be created by mixing between inner zones and outer zones of supernovae is supported by both astrophysical observations and dynamical modelling. An observational example comes from SN 1987A, the most extensively studied supernova to date, an SN II of a star with a main sequence mass in the range 16 - 22 $M_{\odot}$ (Arnett et al. 1989). Based on the evolution of the light curves of iron group elements in SN 1987A, Spyromilio et al. (1990) and Li et al. (1993) concluded these elements were concentrated in high velocity 'bullets' emanating from the core of the supernova. Dynamical modelling of such explosions show that 'fingers' of material from deep within the supernova reach out and separate to form clumps that travel through the outer zones (Hammer et al. 2010). Kifonidis et al. (2003) produced 2-d simulations of core collapse supernovae that showed that the He rich zones slow and act like impenetrable walls that captures the clumps from the interior. However, in the 3-d simulations of Hammer et al. (2010) the clumps of 'bullets' from the inner zones (Ni, Si/S) travel faster and overtake those of the middle O-rich zones, with the fastest penetrating deep into the outermost H zone.

We have examined the isotopic consequences of this mechanism by mixing homogenised compositions of 'bullets' from the inner zones into the outer zones. To produce the component of Ni isotope heterogeneity evident in bulk Solar System objects requires the mass-cut to occur at the base of the Si/S zone. This is because the Ni zone contains significant amounts of stable Ni isotopes which perturb the signature ^{58}Ni of the the Si/S zone. As discussed by Rauscher et al. (2002) the location of the mass-cut is a point of some uncertainty and it may be justified to locate it at the base of the Si/S zone. Another possibility is that the 'bullets' from the Ni zone have so much energy that they are not captured by the H zone and are lost to space (e.g. Burrows et al. 1995). Regardless of the mechanism, from its Ni abundance and isotope composition, it is clear the material from the Ni zone is not heterogeneously sampled by bulk meteorites. So taking just the innermost 'bullets' from above the mass-cut, which originate in the Si/S zone, and mixing these into the outer regions of the star it is possible to examine the conditions under which the Ni isotope signature of the Si/S zone will survive.

Taking a bulk, homogenised, composition from the Si/S zone and mixing it progressively with the rest of the supernova from the outside in, the Si/S contribution dominates the averaged Ni isotopic composition after mixing with the H,

He/N and He/C zones, but addition of material from the O rich zones significantly perturbs this averaged signature, see Figures 10(c) and (d). This is interesting because the models for the production of X-grains also requires these O-rich zones to be largely bypassed because they would produce an environment too oxidising for SiC grains to form or for existing grains to survive (Ebel and Grossman 2001).

However, taking the entire Si/S zone and mixing it into the entire outer zones may not be the most realistic scenario, even in these 1-d models. A more realistic and interesting test is to examine lower limit of Si/S zone mixing that produces appropriate Ni isotopic signatures. Mixing as little as 0.5 % of the homogenised Si/S zone into the outer regions of the supernova, down to the base He/N zone, produces an average Ni isotope composition appropriate for the anomalous Solar System component, see fig 10(d). In the Crab Nebula the expanding supernova remnant formed clumps in the outer shells (Hester 2008), which would have resulted in reducing the mass of the outer shells to which the Si/S zone was mixed. In summary, the Ni isotope signature from the central regions (the Si/S zone) is relatively resistant to dilution and the mechanism for its excavation is supported by astronomical observations and astrophysical modelling. Therefore we propose that the Ni isotope signature observed in meteorites is compatible with variable input of material produced near the base of a SN II.

3.2. Neutron-poor anomalies in other iron-group elements

Previous studies of iron peak elements in CAIs (Lee et al. 1978; Jungck et al. 1984; Heydegger et al. 1979; Niemeyer and Lugmair 1980; Niederer et al. 1980; Birck and Lugmair 1988) and bulk meteorites (Rotaru et al. 1992; Trinquier et al. 2009, 2008) have suggested a component enriched in neutron-rich nuclides (^{48}Ca, ^{50}Ti, ^{54}Cr) which apparently contrasts with the findings of this study. Thus we need to consider the implications of this previous work for our inferences.

The history of neutron-rich anomalies can be traced back to early observations of Ca. Significantly, the Solar System as a whole has anomalously abundant ^{48}Ca relative to ^{46}Ca. In either slow or rapid neutron addition processes both ^{48}Ca and ^{46}Ca should be made in at least comparable abundances. Strikingly, an excess and deficit of a ^{48}Ca rich component (without significant variation in ^{46}Ca or other isotopes of Ca) was observed in two so called 'fractionated, with unknown nuclear effects' (FUN) CAIs EK1-4-1 and C1, respectively (Lee et al. 1978). These isotopic

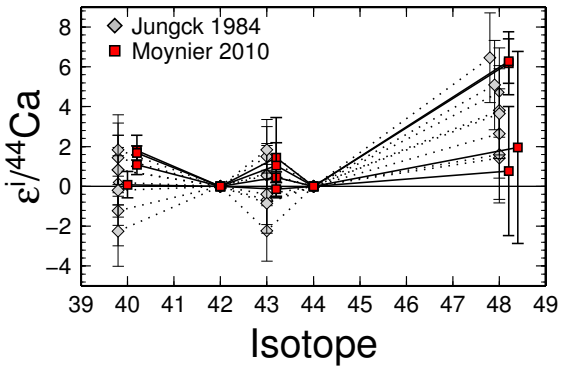

Fig. 11.— Figure showing internally normalised Ca isotope ratios from Jungck et al. (1984) and Moynier et al. (2010). The more precise data determined by Moynier et al. (2010) show anomalies in $\varepsilon^{40}\mathrm{Ca}_{\frac{42}{44}}$ that could not be observed by Jungck et al. (1984). The data from Jungck et al. (1984) have been renormalised to $\varepsilon^{i}\mathrm{Ca}_{\frac{42}{44}}$. Due to their large uncertainties $\varepsilon^{46}\mathrm{Ca}_{\frac{42}{44}}$ have been omitted. Only data for high precision total dissolutions of whole rocks and CAIs have been plotted. A colour version of this figure is available in the online edition.

observations thus led to models which created ^{48}Ca anomalies through neutron-rich nuclear statistical equilibrium (NSE) (Hartmann et al. 1985; Meyer et al. 1996). Neutron rich NSE can also produce other neutron-rich nuclides although the full range of Solar System abundances can only be recreated by mixing material produced over a range of different conditions, the multi-zone mixing process of Hartmann et al. (1985).

Given more recent high-precision isotopic measurements of bulk meteorites, it is now clear that the FUN CAIs do not carry the right isotopic signature to explain the large-scale mass-independent isotopic variability in the Solar System. For example, the Ti isotopic anomalies of the FUN inclusions reported by Niederer et al. (1985) do not correspond to those observed in bulk chondrites by Trinquier et al. (2009). The evidence for Ca anomalies solely on ^{48}Ca in normal CAIs is more equivocal as the literature on normal CAIs show a divergence in results, see Figure 11. Niederer and Papanastassiou (1984) found only hints of anomalies, whereas Jungck et al. (1984) found clear ^{48}Ca anomalies with all other isotope ratios normal (albeit with ± 50 ‰ errors on ^{46}Ca). However, more recently Moynier et al. (2010) have found $\varepsilon^{40}\mathrm{Ca}_{\frac{42}{44}}$ anomalies, unrelated to radioactive decay, in addition to $\varepsilon^{48}\mathrm{Ca}_{\frac{42}{44}}$ anomalies. This more recent work suggests that Ca may have both neutron-rich and neutron-poor anomalies and implies that the history of anomalous Ca may be more complex than simply variable input of ^{48}Ca.

There are undoubtedly anomalies on the neutron-rich ^{50}Ti, as determined in normal CAIs and bulk rock samples by double spiking (Niederer et al. 1985). However, as discussed earlier the variability in the Ti isotopic signature of bulk Solar System material can be produced in the O/Ne zone and neutron-rich NSE need not be invoked. The case for Cr is interesting as internally normalised, mass-independent Cr isotope ratios are traditionally expressed as ^{54}Cr anomalies, normalising to ^{50}Cr/^{52}Cr, but it must be noted that an anomaly in ^{54}Cr is equivalent to an anomaly in ^{50}Cr. We suggest that the inference of ^{54}Cr anomalies may have stemmed from the prior discovery of neutron-rich nuclides in Ti and Ca. To date, no absolute Cr stope ratios have been published. However, by combining data from Trinquier et al. (2007); Trinquier et al. (2008) with the recent mass-dependent isotopic determinations of Moynier et al. (2011b) an approximation can be made, see figure 12. While not ideal, as the mass-dependent and mass-independent compositions were determined during different studies, they give the best available opportunity to investigate the possibility of ^{50}Cr anomalies. From this combination of data, it is apparent that the CI chondrites, which have the largest ^{54}Cr mass-independent anomaly are also most enriched in ^{50}Cr suggesting at least some component of the variation in Cr isotope anomalies may be in ^{50}Cr.

On the other hand, Dauphas et al. (2010) Qin et al. (2011) have recently identified pre-solar grains with large ^{54}Cr excess. Nevertheless, there have been many pre-solar grains identified with highly anomalous Ti compositions (e.g. Ireland 1990; Alexander and Nittler 1999; Zinner 1998, 2003; Hoppe et al. 2010) yet variable proportions of the grains so far identified cannot account for the variations in bulk meteorites. In fact, there is a hint that the pre-solar compositions measured by Ireland (1990) in hibonites could be a candidate for the carrier of Ti isotope anomalies, but it remains that the majority of pre-solar grains so far identified do not play a significant role in the bulk meteorite variation. Moreover, as with Ti, a neutron-rich Cr composition does not require NSE and can be readily produced in a SN II (Qin et al. 2011).

In summary, we question the evidence for the dominant role of a component produced by neutron-rich NSE in causing the mass-independent variability of bulk meteorite samples and normal CAIs. We suggest that the casting of some iron peak mass-independent ratios as neutron-rich anomalies may more reflect the paradigm set by earlier work on FUN inclusions than a necessary implication of the data.

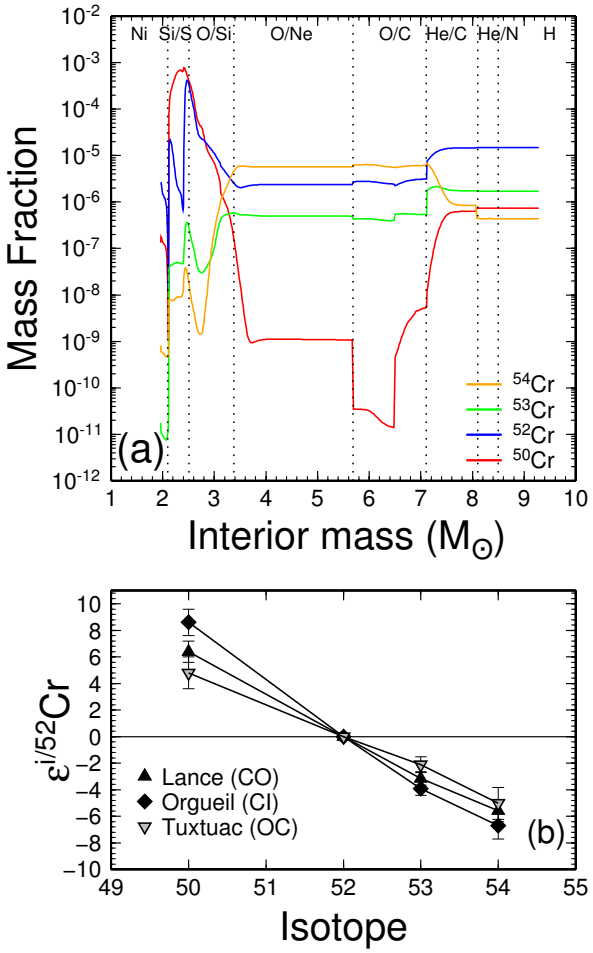

Fig. 12.— (a) Production of Cr isotopes through a 25 $M_{\odot}$ SN II. Data from Rauscher et al. (2002). A colour version of this figure is available in the online edition. (b) Absolute Cr isotope ratios estimated by combining mass-dependent fractionation taken from the $^{50}Cr/^{52}Cr$ of Moynier et al. (2011b) and the and mass-independent data from Trinquier et al. (2007) and Trinquier et al. (2008). As no absolute Cr isotope ratios have yet been published these estimates give the best available indication of the location of Cr isotope anomalies. Orgueil and Lance were processed using data specific to each meteorite from both studies, however, Tuxtuac was only measured by Moynier et al. (2011b) so average OC compositions were used from Trinquier et al. (2007).

3.3. Processing in the early Solar System: Incomplete homogenisation or unmixing?

Input from the component from an SN II as identified above is heterogeneously distributed within the Solar System, see Figures 1 and 5. Different meteorite

groups are thought to have formed in different regions of the early Solar System; they span a large range of heliocentric distances from the ECs closer to the Sun at <1 AU to the CCs further from the Sun at up to 4 AU (e.g. Wood 2005; Andreasen and Sharma 2007; Ciesla 2008). Thus the range of Ni isotope anomalies between different meteorite groups, shown in Figure 1, is evidence for Ni isotope heterogeneity on a large-scale in the early Solar System.

It has previously been suggested that such large scale isotope heterogeneity is due either to incomplete mixing of an anomalous component (e.g. Lee et al. 1979), or unmixing of previously homogeneously distributed components (e.g. Trinquier et al. 2009).

An important additional consideration for any model of Solar System heterogeneity is that the magnitude, or indeed presence, of mass-independent isotopic variability in bulk samples is quite contrasting in elements influenced by similar nucleosynthetic processes. Thus, for iron group elements the are large bulk isotopic anomalies in Ti and Cr (e.g. Leya et al. 2008; Trinquier et al. 2009; Trinquier et al. 2007), smaller variations in Ni (e.g. Dauphas et al. 2008; Regelous et al. 2008; Steele et al. 2011), but no anomalies have yet been documented in bulk samples for Fe or Zn (Dauphas et al. 2008; Moynier et al. 2009). Similarly there are striking differences in the bulk, mass-independent isotopic compositions of Mo (Dauphas et al. 2002a), but barely perceptible anomalies in the neighbouring Zr (Schönbächler et al. 2002; Akram et al. 2011) and none in the nucleosynthetically similar Os (Yokoyama et al. 2007). Yet sequential leaches of the primitive meteorites yield marked differences in mass-independent Zr and Os isotope ratios (Schönbächler et al. 2005; Yokoyama et al. 2010), as is also the case for Mo (Dauphas et al. 2002b). Whilst exotic material seems widely present, as is also evident in the record of pre-solar grains, it is not always distributed evenly between different meteorite groups. We suggest that the different physical properties of the mineralogical hosts of isotopic anomalies of different elements, may result in variable susceptibility to sorting processes in the solar nebula. This means that it may be important to consider not only the isotopic anomalies produced by mixing from a particular supernova zone, but also the phase in which elements of interest condense. For example, we noted that Ni but not Ti isotopic variations in bulk meteorites can be generated by a component from the Si/S zone. If Ni and Ti from the Si/S zone condense into different phases, we can invoke that the Ni bearing phase was sorted in the early solar nebula, but the Ti bearing phase from this zone remained homogeneously distributed. The converse would be true of material

601 from the O/Ne zone. We would likewise argue that the host phases of the ^{96}Zr
602 and ^{186}Os isotope anomalies did not suffer differential sorting in the nebula.

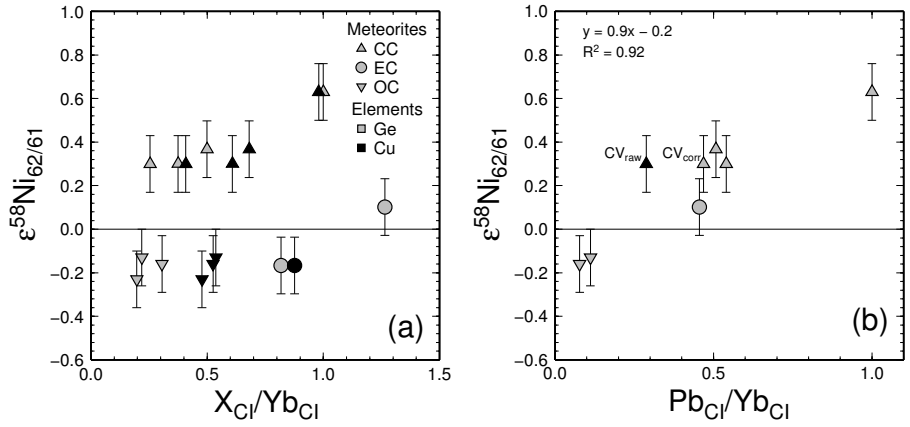

Fig. 13.— Plots showing the correlation between $\varepsilon^{58}\mathrm{Ni}_{\frac{62}{61}}$ and elemental ratios in bulk chondrites. (a) shows that the single monotonic correlation observed by Trinquier et al. (2009) between $\varepsilon^{54}\mathrm{Cr}_{\frac{52}{50}}$ and $\mathrm{Ge_{CI}/Yb_{CI}}$ and $\mathrm{Cu_{CI}/Yb_{CI}}$ in the matrices of CCs form two correlations when the data are extended through the OCs and ECs. (b) shows a single monotonic correlation does exist between $\varepsilon^{58}\mathrm{Ni}_{\frac{62}{61}}$ and $\mathrm{Pb_{CI}/Yb_{CI}}$. $\mathrm{CV_{raw}}$ is the raw abundances ratio Pb/Yb in CV chondrites, whereas $\mathrm{CV_{corr}}$ is that with the CAI component removed. CV CCs contain significant proportions of CAIs which perturb the refractory element concentrations (e.g. Yb). This should not be a significant consideration for other chondrite groups as they contain do not contain such high proportions of CAIs. Proportions and compositions for this correction from Grossman and Ganapathy (1976b,a); McSween Jr. (1977); Grossman et al. (1979).

603 Possible supporting evidence that processing within the Solar System resulted
604 in sorting of anomalous components was found by Trinquier et al. (2009) who
605 noted that variations in $\varepsilon^{54}\mathrm{Cr}_{\frac{52}{50}}$ were correlated with the abundance of moderately
606 volatile elements to refractory elements in the matrices of CC. These elemental
607 ratios are thought to be indices of volatile depletion - processing which occurred
608 to varying extents at different heliocentric distances in the Solar System (e.g.
609 Wasson and Chou 1974; Bland et al. 2005). Trinquier et al. (2009) suggested
610 that these correlations are indicative of preferential removal of previously well-
611 mixed amorphous silicates which contained $\varepsilon^{54}\mathrm{Cr}_{\frac{52}{50}}$ anomalies. This scenario was
612 particularly favoured by the authors because the neutron-rich ^{50}Ti anomaly was not
613 thought to be produced in the same environment as the neutron-poor ^{46}Ti anomaly.
614 By unmixing previously homogeneously distributed anomalies during processing
615 within the Solar System the authors could reconcile correlated anomalies from
616 different nucleosynthetic environments. We have shown that by considering effects
617 on all Ti isotopes, including the normalising isotopes, the anomalies observed in

meteorites can be produced by one SN II event, which may mean processing within the Solar System is not necessary to explain correlation of $\varepsilon^{46}\mathrm{Ti}_{\frac{49}{47}}$ vs. $\varepsilon^{50}\mathrm{Ti}_{\frac{49}{47}}$ but maybe necessary for correlation with other elements.

Trinquier et al. (2009) only plotted a correlation between Ge/Yb and Cu/Yb in CCs, using chemical data from Bland et al. (2005). To extend these correlations to other chondrite groups we have used equivalent data for bulk chondrites from Wasson and Kallemeyn (1988) and Kallemeyn et al. (1994). The correlations with Cu/Yb and Ge/Yb against $\varepsilon^{58}\mathrm{Ni}_{\frac{62}{61}}$ are shown in Figure 13(a). These correlations are not continuous through all the chondrite groups; they in fact form two correlations, one comprising the CCs and the other OCs and ECs.

For the relative abundance of the more volatile element Pb, however, there is a single continuous correlation with ^{58}Ni. These observations have some resonance with the co-variations of the Ni isotopes themselves. Notably $\varepsilon^{62}\mathrm{Ni}_{\frac{58}{61}}$ and $\varepsilon^{64}\mathrm{Ni}_{\frac{58}{61}}$ co-vary through all the chondrite groups, whereas in a plot of $\varepsilon^{60}\mathrm{Ni}_{\frac{58}{61}}$ vs. $\varepsilon^{62}\mathrm{Ni}_{\frac{58}{61}}$ the CC and OC/EC form two different arrays. We would attribute this to $\varepsilon^{60}\mathrm{Ni}_{\frac{58}{61}}$ anomalies being carried by a phase with different physical properties to that of the ^{58}Ni host. Indeed the sulphide phases with large $\varepsilon^{60}\mathrm{Ni}_{\frac{58}{61}}$ excesses identified by Tachibana and Huss (2003) could be a suitable candidate. Regardless of the details, the observations in Figures 13 and 3 indicate that the production of isotopic variation requires something more complex than a single mechanism such as thermal processing.

There are several interesting mechanisms by which radial grain size sorting may occur result from interaction between material in the disk and radiation from the proto-star, namely: photophoresis, radiation pressure and Poynting-Robertson drag. Some combination of these processes may account for the range of observations noted above. Photophoresis is the force exerted on an illuminated particle in a gas rich environment due to differential temperatures of evaporation of gas molecules on the illuminated versus non-illuminated side; molecules on the illuminated side will evaporate with higher temperatures, and so velocities, causing greater momentum transfer (Krauss and Wurm 2005; Wurm et al. 2010).

Radiation pressure is the force exerted on an object being exposed to electromagnetic radiation from the Sun by transfer of momentum from solar photons (Burns et al. 1979). Poynting-Roberston drag is momentum loss that occurs due to re-radiation of energy from a moving particle (Robertson 1937; Burns et al. 1979). Burns et al. (1979) find that over a relatively narrow size range, 0.02 -

2 μm, for particles composed of iron, magnetite and graphite radiation pressure exceeds gravity as the dominant force, while at larger and smaller sizes or less metalloid compositions Poynting-Roberston drag and gravity are more significant. These effects could clearly be significant in redistributing isotopically anomalous supernova grains with high metal content, while other grains would may be the wrong size or composition. These mechanisms might explain why some elements are heterogeneously distributed and others are homogenous.

3.4. Live ^{60}Fe and Variation in $\varepsilon^{60}Ni_{\frac{62}{61}}$

Iron-60 decays to ^{60}Ni with a half-life of 2.62 $\pm$ 0.04 Ma (Rugel et al. 2009) and is of interest as an early Solar System chronometer and a heat source for planetesimal melting. Studies of chondritic components by secondary ion mass spectrometer (SIMS) have suggested that there may have been a significant level of live ^{60}Fe in the early Solar System up to 5×10^{-6} in $^{60}Fe/^{56}Fe_0$ (Tachibana et al. 2006; Guan et al. 2007; Tachibana et al. 2007). However, recent high precision studies of chemically purified mineral separates from differentiated achondrites and CB CCs show that the level of live ^{60}Fe must have been significantly lower, in the range 3×10^{-9} to 2×10^{-8} (Quitté et al. 2010; Quitté et al. 2011; Moynier et al. 2011a).

A somewhat crude test of the level of live ^{60}Fe can be obtained from our bulk dataset. Chondrites all have roughly the same Fe/Ni (16.5 to 18.1), therefore, they cannot distinguish between the effects of live or fossil ^{60}Fe, but iron meteorites have a large range of Fe/Ni, 4.8 to 16.7 (Regelous et al. 2008). Chondrite groups can be linked with iron meteorite groups based on similar nucleosynthetic isotopes anomalies (e.g. $\varepsilon^{62}Ni_{\frac{58}{61}}$). This was suggested by Regelous et al. (2008) and is based on the assumption that meteorites with similar nucleosynthetic anomalies are derived from similar precursor material, so would have received similar budgets of various components, for example the carrier of extant or extinct ^{60}Fe and the source of stable isotope heterogeneity. Therefore, the ranges of Fe/Ni in iron meteorites can be used to make prediction of the deficits in $\varepsilon^{60}Ni_{\frac{58}{61}}$ that should be present if live ^{60}Fe was present at the time of their formation. By comparing these with the observed deficits it is possible to determine the maximum allowable $^{60}Fe/^{56}Fe_0$. In our new dataset we have better defined the links between some chondrite-iron meteorite groups: CV and CO CCs are coupled with the IVB irons

and the OCs are coupled with the IIAB, IIIAB, IVA iron groups. Our higher-precision also makes it worthwhile revisiting the approach of Regelous et al. (2008) to place constraints on $^{60}Fe/^{56}Fe_0$.

The largest difference in Fe/Ni ratios is between the group IVB irons (Fe/Ni 4.8) and the CV and CO chondrites (Fe/Ni $\sim$ 17). Assuming an initial $^{60}Fe/^{56}Fe_0$ of 1×10^{-6} Tachibana et al. (e.g. 2006); Guan et al. (e.g. 2007) a significant deficit of 0.35 ‰ would be expected for the IVB irons if they differentiated from a CO- or CV-like parent body, which would have appropriate $\varepsilon^{62}Ni_{\frac{58}{61}}$. From Figure 3 this clearly is not present. The weighted mean in $\varepsilon^{60}Ni_{\frac{58}{61}}$ of the CV/CO CCs is -0.096 $\pm$ 0.018 ‰, while the weighted mean of the IVB irons is -0.126 $\pm$ 0.009 ‰. This implies a $^{60}Fe/^{56}Fe_0$ of 7.5 $\times10^{-8}$ with a maximum of 1.4 $\times10^{-7}$. Thus our bulk data is in agreement with the findings of Quitté et al. (2010). Quitté et al. (2011) and Moynier et al. (2011a) find that the level of live ^{60}Fe in the material from which the chondrites and irons formed was lower than previously thought. This low level of ^{60}Fe is compatible with the finding of neutron-poor mass-independent stable isotope anomalies and the suggestion that it results from an SN II. Iron-60 is the most neutron-rich Fe isotope with a long half-life; it is the equivalent of ^{64}Ni in the Ni system. A likely scenario for the origin of stable isotope heterogeneity in the early Solar System is that it represents input of the last source to be added. If the nucleosynthetic source were neutron-rich NSE in a SN Ia, for example, then the level of ^{60}Fe would be significantly above the galactic background.

4. Summary and Conclusions

Nickel isotopic compositions have been determined for a variety of chondrite groups and show a range of 0.15, 0.29 and 0.84 ‰, in $\varepsilon^{60}Ni_{\frac{58}{61}}$ $\varepsilon^{62}Ni_{\frac{58}{61}}$ and $\varepsilon^{64}Ni_{\frac{58}{61}}$, respectively. Interestingly, the EH ECs alone match the terrestrial Ni isotope composition. A strong correlation is observed between $\varepsilon^{62}Ni_{\frac{58}{61}}$ and $\varepsilon^{64}Ni_{\frac{58}{61}}$ with slope of the 3.003 $\pm$0.166, which is within error of the slope expected from anomalies in ^{58}Ni. This hypothesis is supported by measurements of the absolute Ni isotope ratio of two samples that span a wide range in $\varepsilon^{62}Ni_{\frac{58}{61}}$ and $\varepsilon^{64}Ni_{\frac{58}{61}}$, Orgueil and Butsura, which show well resolved anomalies in ^{58}Ni and no resolvable mass-independent effects in either ^{62}Ni or ^{64}Ni. Therefore based on these absolute ratios it seems likely that Ni isotope anomalies reside on the neutron-poor isotope ^{58}Ni and not the neutron-rich isotopes ^{62}Ni and ^{64}Ni. In $\varepsilon^{62}Ni_{\frac{58}{61}}$ and $\varepsilon^{64}Ni_{\frac{58}{61}}$, as with

719 other isotope system (e.g. $\varepsilon^{54}Cr_{\frac{52}{50}}$), the CCs show the largest positive anomalies,
720 ECs show approximately terrestrial ratios and OCs have negative anomalies. As
721 previously reported by Regelous et al. (2008) there is no overall correlation between
722 $\varepsilon^{60}Ni_{\frac{58}{61}}$ and $\varepsilon^{62}Ni_{\frac{58}{61}}$.

723 We have examined the effects of mixing small fractions of the average com-
724 positions of various nucleosynthetic environments (SN Ia, SN II, AGB and Wolf-
725 Rayet star) into the Solar System. These results have been compared with the
726 slope of the correlation observed in meteorite samples which describes the large-
727 scale heterogeneity in the early Solar System. Bulk addition of material from
728 the nucleosynthetic environments investigated cannot reproduce the correct slope
729 in $\varepsilon^{64}Ni_{\frac{58}{61}}$ vs. $\varepsilon^{62}Ni_{\frac{58}{61}}$ isotope space by generating ^{58}Ni anomalies, except for one
730 SN Ia model which cannot simultaneously account for the heterogeneity observed
731 in Ti isotopes.

732 Investigation of individual shells of SN II provides a more promising source
733 for the isotopic heterogeneity observed in Ni and possibly other iron group el-
734 ements (Ti and Cr). The Si/S zone of all masses that have been modelled by
735 Rauscher et al. (2002) can produce the correct slope in $\varepsilon^{64}Ni_{\frac{58}{61}}$ vs. $\varepsilon^{62}Ni_{\frac{58}{61}}$ isotope
736 space by overproduction of ^{58}Ni. Importantly, the O/Ne zone can produce ap-
737 proximately the Ti isotope signature observed in the Solar System, i.e. correlated
738 $\varepsilon^{46}Ti_{\frac{49}{47}}$ and $\varepsilon^{50}Ti_{\frac{49}{47}}$ with no anomalies in $\varepsilon^{48}Ti_{\frac{49}{47}}$. This is an important observa-
739 tion as previously it was thought this signature required multiple nucleosynthetic
740 events (Trinquier et al. 2009). Moreover, the Ti isotope signature can be provided
741 by the same nucleosynthetic event that can provide Ni isotope heterogeneity to the
742 Solar System. The Si/S zone overproduces ^{50}Cr relative to the other Cr isotopes,
743 potentially implying that ^{50}Cr anomalies and not ^{54}Cr anomalies should exist in
744 bulk meteorites. The hypothesis of neutron-poor isotope anomalies is supported
745 by observations of anomalies in $\varepsilon^{40}Ca_{\frac{42}{44}}$ (Simon et al. 2009; Moynier et al. 2010).
746 These observations are of particular significance because ^{40}Ca was used for nor-
747 malisation in early measurements on which the initial assumption of neutron-rich
748 anomalies was based (Lee et al. 1978; Niederer and Papanastassiou 1984).

749 The specific mechanism by which inherited nucleosynthetic components are
750 turned into mass-independent isotopic anomalies in bulk Solar System materials re-
751 mains unexplained. Two simple scenarios are possible: incomplete homogenisation
752 of anomalous material in the proto-solar nebula and unmixing of anomalous ma-
753 terial from a previously well-mixed molecular cloud during nebula formation and

processing. The finding that some elements exhibit large anomalies in chondritic components, but none in the bulk, strongly suggests that an important control on the presence of isotopic anomalies is the susceptibility of carrier grains to Solar System processing (e.g. Zr and Os, Schönbächler et al. 2003, 2005; Yokoyama et al. 2007; Yokoyama et al. 2010). Further evidence in support of this hypotheses is found from correlations between mass-independent Ni isotope anomalies and elemental ratios which presumably represent proto-solar nebula processing. While continuous correlations between ratios of highly volatile elements over moderately refractory elements initially suggests sorting of volatile components, this is thought to be unlikely because carrier phases of such anomalies from meteorites to the Solar System are thought to be refractory (Fedkin et al. 2010). Therefore, it may be more plausible that the correlations represent related differences in formation age or heliocentric distance of meteorite parent bodies. Some process that radially redistributes some isotopically anomalous grains relative to others could explain the variation of isotopic anomalies in most elements observed in meteorites. Three possible processes are photophoresis, radiation pressure and Ponyting-Roberston drag, or some combination, acting on grains differentially (Krauss and Wurm 2005; Wurm et al. 2010; Mukai and Yamamoto 1982; Jackson and Zook 1992; Burns et al. 1979). The lack of correlation of $\varepsilon^{60}\mathrm{Ni}_{\frac{62}{61}}$ and $\varepsilon^{58}\mathrm{Ni}_{\frac{62}{61}}$ anomalies is probably due to differential mixing of grains rich in fossil ^{60}Fe and grains with nucleosynthetic Ni isotope anomalies.

Acknowledgments

We are grateful to Derek Vance (BIG), Vyllinniskii Cameron (BIG) and Matthias Willbold (BIG) for advice and technical assistance, Sara Russell (NHM) and Caroline Smith (NHM) for helpful discussion and meteorite samples. We gratefully acknowledge a NERC studentship to RCJS (NE/F007329/1) and additional support from STFC (ST/F002734/1) and NHM which made this work possible. We thank the anonymous reviewer for their helpful comments which improved the manuscript and Frank Timmes for his editorial handling.

A. Appendix

A.1. Mass-independent method

The chemical separation and mass spectrometric techniques used to acquire the data presented in this paper have been described in some detail in a previous study (Steele et al. 2011), but a brief summary below outlines the main features of the procedure. After dissolution using a standard HF-HNO_3 method, Ni was separated from terrestrial and meteorite samples using a four column ion exchange procedure. The first column used the highly Ni specific reagent dimethylglyoxime (DMG), dissolved in a weak HCl-acetone solution, to elute Ni from a BioRad AG 50 column. This column separated Ni from the majority of the matrix and was performed twice. Subsequent columns reduced to the level of the blank acid the specific matrix components known to hinder Ni isotope analyses: Eichrom TRUspec to remove Fe which is an interference on ^{58}Ni, BioRad AG 50 to remove P and residual organics from breakdown of DMG and TRUspec, BioRad AG MP 1 to reduce the ^{64}Zn interference on ^{64}Ni. The yield of the chemical separation procedure was determined to be within error of 100 %.

The isotopic composition of Ni separated from meteorites by this method was then determined using a Neptune multiple-collector inductively-coupled plasma mass spectrometer (MC-ICP-MS) in medium resolution ($M/\Delta M \geq 6000$) in order to resolve the minor molecular interferences present in the Ni mass range. Samples were introduced via a Cetac Aridus desolvating nebuliser, with a $\sim$50 μLmin^{-1} nebuliser tip. The interferences from ^{58}Fe on ^{58}Ni and ^{64}Zn on ^{64}Ni were reduced by effective chemical separation (see above) and corrected by peak stripping to a level where data accuracy was not affected. The Faraday cups collecting the ^{58}Ni and ^{60}Ni beams were connected to amplifiers fitted with 10^{10} Ω feedback resistors, allowing the precision limiting intensities of the minor isotopes to be increased to >40 pA whilst simultaneously collecting all isotopes. This high beam intensity on ^{64}Ni also helped minimise the influence of the Zn interference. Samples were analysed at least 4 times in one analytical session, each analysis comprising 100 measurements of $\sim$8.4 s. On-peak blank measurements bracketed every analysis of every sample or standard and were subtracted. Samples were internally normalised to a ^{58}Ni/^{61}Ni ratio of 59.722 (Gramlich et al. 1989a,b) and are presented as ε units calculated relative to NIST SRM 986 (Gramlich et al. 1989a,b) which was used as a bracketing standard for external normalisation. These analyses yield typical precisions of 0.03, 0.05 and 0.08, ‰ (2 s.e. n $\geq$4) for $\varepsilon^{60}\mathrm{Ni}_{\frac{58}{61}}$, $\varepsilon^{62}\mathrm{Ni}_{\frac{58}{61}}$ and $\varepsilon^{64}\mathrm{Ni}_{\frac{58}{61}}$,

where $\varepsilon^{i}\mathrm{Ni}_{\frac{k}{j}}$ is the parts per ten thousand difference from a standard of the ratio i/j internally normalised to k/j in this case $^{58}\mathrm{Ni}/^{61}\mathrm{Ni}$. This precision is comparable to the reproducibility of multiple dissolutions of the same sample.

A.2. York regression of meteorite samples

York regressions (York et al. 2004) on $\varepsilon^{64}\mathrm{Ni}_{\frac{58}{61}}$ *vs.* $\varepsilon^{62}\mathrm{Ni}_{\frac{58}{61}}$ for the 30 meteorite and peridotite samples (spallation-affected Tlacotepec was omitted) were performed in three different ways as follows: a) using the 215 individual analyses for which all 5 isotopes were measured, table A.1 (given in full in the online supplementary data), b) using the 30 sample means and their homoscedastic standard errors (h.s.e.) explained in more detail in section A.2.1 but in essence uncertainties are obtained using all analyses of all samples rather than just those for individual samples (see also Steele et al. 2011), and c) using the 30 sample means and their standard errors (s.e.) (i.e. Table 1 main text). Table A.2 summarises the results of the regressions. Details of how the errors and error correlations were calculated for each regression are given in sections A.2.1 to A.2.3.

Sample	$\varepsilon^{62}\mathrm{Ni}_{\frac{58}{61}}$	1 s.d.	$\varepsilon^{64}\mathrm{Ni}_{\frac{58}{61}}$	1 s.d.
JP-1_004	0.068	0.042	0.106	0.082
JP-1_016	0.017	0.042	0.120	0.082
JP-1_028	0.028	0.042	0.084	0.082
JP-1_040	-0.002	0.042	0.141	0.082
JP-1_004	0.047	0.042	0.193	0.082
JP-1_008	0.019	0.042	0.121	0.082
JP-1_012	0.017	0.042	0.148	0.082
JP-1_016	0.026	0.042	0.055	0.082
JP-1_020	0.040	0.042	0.088	0.082
JP-1_004	0.050	0.042	0.131	0.082

Table A.1: Table showing the first 10 examples of the 215 analyses for which all 5 isotopes were measured. The correlation coefficient between the errors in $\varepsilon^{62}\mathrm{Ni}_{\frac{58}{61}}$ and $\varepsilon^{64}\mathrm{Ni}_{\frac{58}{61}}$ is 0.68. This table is published in its entirety in the electronic edition of the Astrophysical Journal. This portion is shown here for guidance regarding its form and content.

From Table A.2 we see that the slopes (a) and (b) are in excellent agreement and both have acceptable MSWDs. We choose to report (a) in the main text for simplicity, i.e., there are fewer steps to the data reduction and the method is easier to understand. Method (b), however, benefits from 8, 12, and 8 additional

measurements of $\varepsilon^{62}\mathrm{Ni}_{\frac{58}{61}}$ on samples Bristol, Santa Clara and JP-1 respectively which, because there are no accompanying $\varepsilon^{64}\mathrm{Ni}_{\frac{58}{61}}$ data, cannot be included in (a).

					Monte-Carlo Simulated	
	n_Υ	Slope	Slope Error (2σ)	MSWD	Slope Error (2 s.d.)	MSWD
(a)	215	3.003	0.166	1.021		
(b)	30	2.982	0.177	1.341	0.179	1.009
(c)	30	2.824	0.133	1.832	0.229	1.459

Table A.2: York regression (York et al. 2004) of $\varepsilon^{64}\mathrm{Ni}_{\frac{58}{61}}$ *vs.* $\varepsilon^{62}\mathrm{Ni}_{\frac{58}{61}}$ for all meteorite samples, except Tlacotepec, and the two peridotites JP-1 and DTS-2. n_Υ is the number of data points used in the regression. (a) Individual analyses with errors of 0.042 and 0.082 (1σ) for $\varepsilon^{62}\mathrm{Ni}_{\frac{58}{61}}$ and $\varepsilon^{64}\mathrm{Ni}_{\frac{58}{61}}$ respectively and error correlation 0.68; (b) sample means with homoscedastic standard errors; (c) sample means with standard errors. For (b) and (c) the correlation used is given by equation A8. The rightmost two columns give slope errors and MSWD for regressions (b) and (c) estimated from a Monte-Carlo simulation. See appendix main text for further details.

Regression (c) gives a different slope, albeit within error, and an MSWD of 1.7 which suggest the data are not from populations whose means lie on a straight line. We argue that (b) is preferred over (c) because the assigned errors are more robust in the former and that the high MSWD of (c) is to be expected. Intuitively, this is plausible as one might anticipate that the standard error may give over- and underestimates of the true error purely by chance when the number of repeat analyses is small and, furthermore, that the *underestimates* may have a greater influence on both the slope and MSWD than the overestimates. This has been confirmed by Monte-Carlo simulation.

Firstly, we tested our Monte-Carlo simulation code using a dataset taken from Albarède (1995, Table 5.23, p304). The same data were used by York (York et al. 2004, table II, dataset 4) to compare the slope and intercept errors of the regression algorithm to that given by the simulation. Our York regression implementation gave a slope error in agreement with York et al. (2004) to the six decimal places published and an intercept error of 0.012985 compared to 0.012981. The relative difference from the Monte-Carlo simulated errors are 0.007% (slope) and 0.006% (intercept) in our simulation of 10^8 trials compared to 0.037% and 0.037% respectively given by York's simulation (York et al. 2004) using 10^7 trials.

Monte-Carlo simulation of regression (c) is carried out as follows.

1. The York regression through the measured data is calculated to yield the

860 least-squares adjusted data points or expectation values, see (York et al.
861 2004).

862 2. Taking the expectation values in (1) as population means for each sample
863 and using standard deviations of 0.042 and 0.082 for $\varepsilon^{62}\mathrm{Ni}_{\frac{58}{61}}$ and $\varepsilon^{64}\mathrm{Ni}_{\frac{58}{61}}$
864 respectively and a correlation of 0.68, from the measured data, simulated
865 data are generated. The number of simulated $\varepsilon^{62}\mathrm{Ni}_{\frac{58}{61}}$ and $\varepsilon^{64}\mathrm{Ni}_{\frac{58}{61}}$ data equals
866 that in the measured dataset for each sample.

867 3. The means and standard errors of each sample are calculated from the sim-
868 ulated dataset, as is the correlation using equation A8. Note that we re-
869 calculated r_0 from the simulated data rather than taking a value of 0.68.
870

871 4. York regression is performed using the means, standard errors and correla-
872 tions from (3). The slope, intercept, and MSWD are stored.

873 5. Steps 2–4 are repeated 10^7 times.

874 6. The standard deviation of the slopes and mean value of the MSWD is cal-
875 culated and reported in Table A.2.

876 Monte-Carlo simulation of regression (b) is carried out similarly but with
877 homoscedastic standard errors calculated at step (3) rather than standard errors.
878 The results of these simulations are given in Table A.2. Note that for regression
879 (b) the standard deviation of the simulated slopes, 0.179, is in excellent agreement
880 with the slope error from the regression, 0.177 but this is not so for regression (c).
881 In addition, the simulation of regression (c) gives an MSWD of 1.46 compared to
882 a value close to 1 for regression (b). Hence, a high MSWD is to be expected if
883 standard errors are used for the regression where rather small numbers of repeat
884 analyses are made.

885 *A.2.1. Regression using homoscedastic errors*

886 A homoscedastic dataset is one where the data are drawn from a number
887 of parent populations which may have different population means but share the
888 same population variance. This may occur in practice where, as in the present
889 case, many samples are analysed under essentially identical conditions. Let the

j^{th} analyses of sample i be denoted x_{ij}. Let there be n_{xi} analyses of each sample and a total of N samples. Furthermore, we consider the x_{ij} to be drawn from populations with variance σ_x^2. We can utilise all these data to make an unbiased estimate, s_x^2, of this variance given by Kenney and Keeping (1951, Page 164).

$$s_x^2 = \frac{1}{k_x} \sum_{i=1}^{N} \sum_{j=1}^{n_{xi}} (x_{ij} - \bar{x}_i)^2 \tag{A1}$$

where the sample mean, $\bar{x}_i$, and the number of degrees of freedom, k_x, are given by

$$\bar{x}_i = \frac{1}{n_{xi}} \sum_{j=1}^{n_{xi}} x_{ij} \tag{A2}$$

and

$$k_x = \left(\sum_{i=1}^{N} n_{xi} \right) - N. \tag{A3}$$

Thus, the homoscedastic standard error on the sample mean is

$$\text{h.s.e.} = \frac{s_x}{\sqrt{n_{xi}}}. \tag{A4}$$

Let x and y refer to $\varepsilon^{62}\text{Ni}_{\frac{58}{61}}$ and $\varepsilon^{64}\text{Ni}_{\frac{58}{61}}$ respectively. We use the entire dataset to calculate s_x^2 and s_y^2, rather than only those used in the regression, a total of 375 and 312 analyses for x and y respectively on 36 samples giving $s_x = 0.042$ and $s_y = 0.082$.

In an analogous way, the covariance of the errors, s_{xy}, and their correlation, r_0, are given by

$$s_{xy} = \frac{1}{k} \sum_{i=1}^{N} \sum_{j=1}^{n_i} (x_{ij} - \bar{x}_i)(y_{ij} - \bar{y}_i) \tag{A5}$$

and

$$r_0 = \frac{s_{xy}}{s_x s_y} \tag{A6}$$

where

$$k = \left(\sum_{i=1}^{N} n_i \right) - N. \tag{A7}$$

The sum over j from 1 to n_i in equation A5 includes only those analyses where both x and y are measured; in our case a total of 312 analyses giving $r_0 = 0.68$.

The correlation, r_i, between the means, $\bar{x}_i$ and $\bar{y}_i$, for those samples where every analysis measured both x and y, is simply $r_i = r_0$. However, in the case of samples JP-1, Bristol, and Santa Clara some analyses measured x only. The correlation for these three samples, therefore, needs special treatment and is given by

$$r_i = r_0 \sqrt{\frac{n_{yi}}{n_{xi}}}. \tag{A8}$$

This can be shown as follows. Consider

$$f = au + bw \tag{A9}$$

where a and b are constants. Propagating the errors (denoted by s suitably subscripted) in u and w into f gives,

$$s_f^2 = a^2 s_u^2 + b^2 s_w^2. \tag{A10}$$

Now let v be correlated with u with covariance s_{uv}, but not with w. The covariance between f and v is given by

$$s_{fv} = \frac{\partial f}{\partial u} s_{uv} \tag{A11}$$

$$= a\, s_{uv}. \tag{A12}$$

Replacing the covariances with correlations, r_{fv} and r_{uv}, gives,

$$r_{fv} = a\, r_{uv} \frac{s_u}{s_f} \tag{A13}$$

$$= r_{uv} \sqrt{\frac{a^2 s_u^2}{a^2 s_u^2 + b^2 s_w^2}} \tag{A14}$$

where we have substituted s_f from equation A10.

If we have n correlated measurements of x and y, giving means $\bar{x}_n$ and $\bar{y}$, and a further m measurements of x with mean $\bar{x}_m$ then $\bar{x}$, the mean of all $n + m$ measurements of x, is given by

$$(n + m)\bar{x} = n\bar{x}_n + m\bar{x}_m. \tag{A15}$$

Equation A15 is identical to equation A9 with $f \to \bar{x}$, $u \to \bar{x}_n$, $w \to \bar{x}_m$, $a \to n/(n + m)$ and $b \to m/(n + m)$. Finally, by substituting $v \to \bar{y}$ and $r_{fv} \to r$, equation A14 becomes

$$r = r_{\bar{x}_n \bar{y}} \sqrt{\frac{n^2 s_{\bar{x}_n}^2}{n^2 s_{\bar{x}_n}^2 + m^2 s_{\bar{x}_m}^2}} \tag{A16}$$

where r is the correlation between the errors in $\bar{x}$ and $\bar{y}$. If the analyses are from a single population, we can use $ns^2_{\bar{x}_n} = ms^2_{\bar{x}_m}$ and equation A16 becomes

$$r = r_{\bar{x}_n\bar{y}}\sqrt{\frac{n}{n+m}}. \tag{A17}$$

Lastly, in the homoscedastic case, we have $r_{\bar{x}_n\bar{y}} = r_0$ and putting $r \to r_i$, $n \to n_{yi}$ and $n + m \to n_{xi}$ completes the proof of equation A8. Table A.3 shows the calculated values of r_i for each sample. Note that the values in columns "n" and "n_{64}" in Table A.3 correspond to n_{xi} and n_{yi} respectively.

A.2.2. Regression using individual analyses

In this case we are constrained to regress only using those analyses for which both $\varepsilon^{62}\mathrm{Ni}_{\frac{58}{61}}$ (x) and $\varepsilon^{64}\mathrm{Ni}_{\frac{58}{61}}$ (y) are measured. We assign errors $s_x = 0.042$ and $s_y = 0.082$ respectively and correlation $r_0 = 0.68$ given by equations A1 and A6 to each analysis.

A.2.3. Regression using standard errors

This may be considered the more conventional approach where the errors used for the regression is the standard error (s.e.) calculated on a sample by sample basis. The sample standard deviation, s_{xi}, and standard error are given by,

$$s^2_{xi} = \frac{1}{n_{xi}-1}\sum_{j=1}^{n_{xi}}(x_{ij} - \bar{x}_i)^2 \tag{A18}$$

$$\text{s.e.} = \frac{s_{xi}}{\sqrt{n_{xi}}}. \tag{A19}$$

The correlation may be calculated similarly on a sample by sample basis thus,

$$r'_i = \frac{\sum_{j=1}^{n_i}(x_{ij} - \bar{x}_i)(y_{ij} - \bar{y}_i)}{\sqrt{\sum_{j=1}^{n_i}(x_{ij} - \bar{x}_i)^2 \sum_{j=1}^{n_i}(y_{ij} - \bar{y}_i)^2}}. \tag{A20}$$

However, for small sample sizes, typically $n_i = 4$ in the present case, r'_i is poorly constrained. This can be demonstrated by a Monte-Carlo simulation of pseudo-random, normally-distributed data pairs with population correlation $\rho = 0.68$.

For $n = 4$, the 95% lower and upper confidence limits on r'_i are -0.66 and $+0.99$ respectively. With such wide confidence limits it may be of little value to include the correlation in the regression at all so we prefer to use the more robust correlation calculated from the entire dataset using equation A8 as we do for the homoscedastic case.

A.3. Mass-dependent method to obtain 'absolute' ratios

Analysis by adding a double spike isotopic tracer (Dietz et al. 1962; Dodson 1963, 1969; Russell 1971) provides a robust method for obtaining the natural mass-dependent isotopic fractionation of elements with 4 or more isotopes. A ^{61}Ni-^{62}Ni double spike technique established in Bristol has been previously described by Cameron et al. (2009). However, the technique of Cameron et al. (2009) was set up to investigate the isotopic fractionations in a large number of samples where the highest precision was not a critical concern. By contrast in the present we require high precision measurements of a small number of samples. We have chosen two samples which span the largest range in $\varepsilon^{64}\mathrm{Ni}_{\frac{58}{61}}$, Orgueil +0.585 and Butsura -0.160. To determine which isotopic abundances vary to produce this 0.9 ‰ difference requires a precision better than 0.45 ‰, whereas (Cameron et al. 2009) report a precision of 0.8 ‰. We have, therefore, adjusted the techniques slightly to re-optimise for higher precision at the expense of sample throughput. The changes are outlined below along with a short discussion of the precision.

A.3.1. Double spike inversion

Double spike inversion for natural mass-dependent fractionation works by adding an isotopic tracer with two highly enriched isotopes to a sample. The ratio of these two isotopes can then be used as an internal standard to correct for instrumental mass fractionation, thus any residual fractionation occurred prior to analysis (e.g. Dodson 1963; Russell 1971). In order to determine the absolute ratios requires the following to be known: (i) the composition of the double spike, (ii) the mass fractionation curve which passes through the sample composition, and (iii) the measured composition of the sample spike mixture. The mass fractionation curve is defined by the exponential (kinetic) mass fractionation law, assumed to be an accurate model of both the instrumental and natural isotopic fractionation, and

	Group	NHM no.	n	n_{64}	$\varepsilon^{60}Ni_{\frac{58}{61}}$	2 h.s.e.	$\varepsilon^{62}Ni_{\frac{58}{61}}$	2 h.s.e.	$\varepsilon^{64}Ni_{\frac{58}{61}}$	2 h.s.e.	r
Carbonaceous Chondrites											
Orgueil	CI	1985, M148	4	4	-0.008	0.025	0.203	0.042	0.585	0.082	0.68
Cold Bokkeveld	CM	1919, 144	4	4	-0.084	0.025	0.113	0.042	0.335	0.082	0.68
Murchison	CM	—	4	4	-0.098	0.025	0.124	0.042	0.298	0.082	0.68
Felix	CO	—	4	4	-0.079	0.025	0.097	0.042	0.262	0.082	0.68
NWA 801	CR	1919, 89	5	5	-0.157	0.022	0.116	0.038	0.361	0.073	0.68
Allende	CV	1988, M23	4	4	-0.098	0.025	0.131	0.042	0.324	0.082	0.68
Leoville	CV	13989	8	8	-0.107	0.018	0.061	0.030	0.135	0.058	0.68
EnstatiteChondrites											
Abee	EH	51366	4	4	-0.007	0.025	0.027	0.042	0.084	0.082	0.68
St. Mark's	EH	1990, 339	4	4	-0.017	0.025	0.039	0.042	0.113	0.082	0.68
Khairpur	EL	992, M7	4	4	-0.023	0.025	-0.054	0.042	-0.049	0.082	0.68
Ordinary Chondrites											
Butsure	H	—	28	28	-0.048	0.009	-0.053	0.016	-0.171	0.031	0.68
Ceniceros	H	1915, 86	4	4	-0.063	0.025	-0.050	0.042	-0.078	0.082	0.68
Barratta	L	1975, M11	4	4	-0.042	0.025	-0.028	0.042	-0.105	0.082	0.68
Tenham	L	—	4	4	-0.026	0.025	-0.057	0.042	-0.117	0.082	0.68
Tieschitz	HL	—	8	8	-0.052	0.018	-0.080	0.030	-0.253	0.058	0.68
Chainpur	LL	—	8	8	-0.054	0.018	-0.065	0.030	-0.171	0.058	0.68
Dhurmsala	LL	—	4	4	-0.049	0.025	-0.085	0.042	-0.210	0.082	0.68
Iron Meteorites											
Coahuila	2AB	54242	4	4	-0.031	0.025	-0.088	0.042	-0.259	0.082	0.68
Henbury	3AB	—	4	4	-0.056	0.025	-0.090	0.042	-0.304	0.082	0.68
Lenarto	3AB	61304	4	4	-0.047	0.025	-0.083	0.042	-0.318	0.082	0.68
Arispe	IC	86425	4	4	-0.049	0.025	-0.129	0.042	-0.317	0.082	0.68
Bendegó	IC	66585	4	4	-0.013	0.025	-0.001	0.042	-0.030	0.082	0.68
Bristol	IVA	1955226	16	8	-0.048	0.013	-0.047	0.021	-0.165	0.058	0.48
Putnam County	IVA	90228	8	8	-0.049	0.018	-0.069	0.030	-0.243	0.058	0.68
Skookum	IVB	—	4	4	-0.129	0.025	0.067	0.042	0.168	0.082	0.68
Cape of Good Hope	IVB	1985,M246	4	4	-0.126	0.025	0.099	0.042	0.271	0.082	0.68
Hoba	IVB	1930976	8	8	-0.122	0.018	0.084	0.030	0.214	0.058	0.68
Santa Clara	IVB	1983,M27	16	4	-0.121	0.013	0.087	0.021	0.369	0.082	0.34
Tlacotepec	IVB	1959913	4	4	-0.136	0.025	0.023	0.042	0.134	0.082	0.68
Terrestrial Samples and Standards											
PtYG	T	—	20	20	0.010	0.011	-0.009	0.019	0.012	0.037	0.68
NiSalt	T	—	16	16	-0.016	0.013	0.058	0.021	0.226	0.041	0.68
CPI	T	—	16	12	0.002	0.013	0.017	0.021	0.083	0.047	0.59
986-Col	T	—	4	4	0.002	0.025	-0.024	0.042	0.000	0.082	0.68
DTS-2	T	—	4	4	-0.007	0.025	0.038	0.042	0.161	0.082	0.68
JP-1	T	—	58	50	-0.006	0.007	0.035	0.011	0.117	0.023	0.63
361	T	—	72	41	-0.011	0.006	0.029	0.010	0.136	0.026	0.51

Table A.3: Sample means of $\varepsilon^{60}Ni_{\frac{58}{61}}$, $\varepsilon^{62}Ni_{\frac{58}{61}}$and $\varepsilon^{64}Ni_{\frac{58}{61}}$ taken from Table 1 (main text) and from Steele et al. (2011). 2 h.s.e. Errors are two standard deviations of the mean based on an assumption of homoscedasticity for the set of individual analyses of all samples and standards analysed during this study, see text for details.

one known composition lying on the curve, **n**. For samples with isotopic anomalies, as in the present case or for Pb isotopes (e.g. Compston and Oversby 1969), a

separate internally normalised measurement of the unspiked sample defines **n**.

Samples were spiked in a ∼1:1 ratio with a ^{61}Ni:^{62}Ni spike in approximate molar proportions 40 % and 60 % following Cameron et al. (2009). The four isotopes used for the inversion were ^{58}Ni, ^{60}Ni, ^{61}Ni and ^{62}Ni.

Analyses were made on the second Thermo Finnigan Neptune MC-ICP-MS (serial no. 1020) in Bristol using an introduction system set up similar to the one used for the mass-independent analyses with Cetac Aridus desolvating nebuliser, 50 μLmin^{-1} nebuliser tip, $\sim$ 10 mLmin^{-1} of N_2. However, the mass spectrometer was set up differently and used low resolution and a different cup configuration. Molecular interferences, e.g. ^{40}Ar^{18}O, were reduced to background levels by use of N_2 and were subtracted by on peak blank correction (see below).

The two samples chosen for double spike analysis (Orgueil and Butsura) were measured multiple times in one analytical session which followed approximately the same analytical protocol as Cameron et al. (2009). At the beginning of the sequence, and interleaved with spiked samples throughout the sequence, a number of unspiked NIST SRM 986 analyses were made which were used to correct for any non-exponential fractionation or other non-exponential effects, for example Faraday cup yield factors. Spiked samples were measured in groups of between three and five analyses, which included: spiked NIST SRM 986 with mixture ratios 0.5, 1 and 2; Orgueil; Butsura in mixture ratios of 1. Spiked meteorites were each analysed 8 times interleaved throughout the analytical session. Two washes were performed after each analysis to clean the spray chamber and on peak blanks were measured after each analysis. Spiked samples, where all isotopes have approximately the same abundance, were run at $\sim$ 200 pA for the most abundant isotope. Approximately 10 μg of sample Ni was consumed in total for each meteorite.

A.3.2. Mass-dependent precision

The results of the 8 repeat measurements of Orgueil and Butsura are given in Table 2 (main text), Table A.4 and Figure 4. These analyses yield an uncertainty for the ^{58}Ni/^{61}Ni ratio of 0.15 - 0.2 ‰ 2 s.e. for the 8 repeat measurements. The uncertainty in the absolute isotope ratios of samples, however, must include errors on both the mass-dependent and mass-independent measurements. This

	$\varepsilon^{58/61}$Ni	$\varepsilon^{60/61}$Ni	$\varepsilon^{61/61}$Ni	$\varepsilon^{62/61}$Ni	$\varepsilon^{64/61}$Ni
Butsura					
i	-3.05	-1.05	0.00	0.93	2.74
ii	-2.95	-1.02	0.00	0.90	2.64
iii	-2.81	-0.97	0.00	0.85	2.51
iv	-2.93	-1.01	0.00	0.89	2.62
v	-2.89	-1.00	0.00	0.88	2.58
vi	-3.02	-1.04	0.00	0.92	2.71
vii	-3.15	-1.08	0.00	0.96	2.83
viii	-3.19	-1.10	0.00	0.98	2.87
Average	-3.00	-1.03	0.00	0.91	2.69
2 s.e.	0.09	0.03	0.00	0.03	0.09
Orgueil					
i	-1.98	-0.66	0.00	0.84	2.47
ii	-2.59	-0.86	0.00	1.04	3.06
iii	-2.27	-0.75	0.00	0.94	2.75
iv	-2.12	-0.70	0.00	0.89	2.61
v	-1.92	-0.64	0.00	0.82	2.41
vi	-2.28	-0.76	0.00	0.94	2.76
vii	-2.11	-0.70	0.00	0.88	2.60
viii	-2.07	-0.69	0.00	0.87	2.56
Average	-2.17	-0.72	0.00	0.90	2.65
2 s.e.	0.15	0.05	0.00	0.05	0.14

Table A.4: Table showing absolute ratios for two meteorites which cover a large range in $\varepsilon^{64}\text{Ni}_{\frac{58}{61}}$. These data show good evidence that for these two samples, and by inference the data set as a whole, contain ^{58}Ni anomalies and not correlated ^{62}Ni and ^{64}Ni anomalies. The uncertainties include contributions from the mass-dependent analyses, mass-independent analyses and the standards used for the second normalisation.

problem needs to be assessed with care as errors in any one isotope used in the double spike inversion can affect all the reported ratios. A more obvious problem is that we do not calculate an error for the ^{58}Ni/^{61}Ni ratio in the mass-independent data as it is the normalising ratio. Thus we undertook a simulation, using a modelled composition with mass-dependent fractionation of zero. These data were processed through the double spike inversion with mass-independent anomalies for each ratio (i.e. $\varepsilon^{60}\text{Ni}_{\frac{58}{61}}$, $\varepsilon^{62}\text{Ni}_{\frac{58}{61}}$ and $\varepsilon^{64}\text{Ni}_{\frac{58}{61}}$) varied randomly around zero in a distribution with a standard deviation (s.d.) equal to that of the uncertainty on the mass-independent data (0.03, 0.05 and 0.08 ‰). We made 5000 inversions to build up a robust model of the uncertainty in the absolute ratios. The results of this simulation are given in Table A.5. They show that the contribution to the uncertainty on the absolute ratio from the precision of the mass-independent data is significant relative to the precision of the mass-dependent and therefore must be included in the uncertainty of the absolute ratios. The uncertainty contribution from the mass-independent measurements (as modelled above) and the uncertainty

	$\varepsilon^{58/61}$Ni	$\varepsilon^{60/61}$Ni	$\varepsilon^{61/61}$Ni	$\varepsilon^{62/61}$Ni	$\varepsilon^{64/61}$Ni
Monte carlo simulation of mass-independent contribution to uncertainty					
Average	0.00	0.00	0.00	0.00	0.00
2 s.d.	0.05	0.01	0.00	0.05	0.10
Contribution to uncertainty from 1:1 standard spike mixtures					
Average	-0.17	-0.06	0.00	0.05	0.16
2 s.e.	0.20	0.06	0.00	0.06	0.19

Table A.5: Top, Table showing the effect of uncertainty on the mass-independent anomaly of samples on the double spike inversion. These data were obtained using Monte Carlo simulation. Bottom, Table showing the uncertainty contribution from the spiked standards used for normalisation and measured during the analytical session.

from the mass-dependent measurement have thus been summed in quadrature to obtain the overall precision of the absolute ratios quoted in Table 2 (main text).

The external reproducibility of analyses made by this technique has been assessed using measurements of NIST SRM 986 spiked in a 1:1 ratio made in seven analytical session over an eighteen month period, kindly provided by Derek Vance and Vyllinniskii Cameron. These analyses yield an error with 2 standard deviations (2 s.d.) of 0.59 somewhat larger than the 2 s.d. of the meteorite data made in a single session ($\sim$0.34 ‰). Thus the contribution to the uncertainty on the absolute ratio from the mass-dependent measurements is more realistically greater by a factor of roughly 2 than that determined from the within run precision (2 s.e. = 0.21 ‰), but this is still sufficient to resolve the 0.9 ‰ difference between meteorites, see section 2.1.

REFERENCES

Akram, W., Schonbachler, M., Williams, H., Halliday, A., 2011. The origin of nucleosynthetic zirconium-96 heterogeneities in the inner solar system. In: *Lunar and Planetary Institute Science Conference Abstracts* . Vol. 42. p. 1908.

Albarède, F., 1995. Introduction to geochemical modeling. *Cambridge University Press.*

Alexander, C. M. O., Nittler, L. R., 1999. The Galactic Evolution of Si, Ti, and O Isotopic Ratios. *The Astrophysical Journal* 519 (1), 222.

1046 Andreasen, R., Sharma, M., 2007. Mixing and Homogenization in the Early So-
1047 lar System: Clues from Sr, Ba, Nd, and Sm Isotopes in Meteorites. *The*
1048 *Astrophysical Journal* 665 (1), 874–883.

1049 Arnett, W. D., Bahcall, J. N., Kirshner, R. P., Woosley, S. E., 1989. Supernova
1050 1987A. *Annual Reviews in Astronomy and Astrophysics* 27, 629–700.

1051 Birck, J. L., Lugmair, G. W., 1988. Nickel and chromium isotopes in Allende
1052 inclusions. *Earth and Planetary Science Letters* 90, 131–143.

1053 Bland, P., Alard, O., Benedix, G., Kearsley, A., Menzies, O., Watt, L., Rogers, N.,
1054 2005. Volatile fractionation in the early solar system and chondrule/matrix
1055 complementarity. *Proceedings of the National Academy of Sciences* 102 (39),
1056 13755–13760.

1057 Burbidge, E. M., Burbidge, G. R., Fowler, W. A., Hoyle, F., 1957. Synthesis of
1058 the Elements in Stars. *Reviews of Modern Physics* 29 (4), 547–650.

1059 Burns, J., Lamy, P., Soter, S., 1979. Radiation forces on small particles in the
1060 Solar System. *Icarus* 40 (1), 1–48.

1061 Burrows, A., Hayes, J., Fryxell, B., 1995. On the nature of core-collapse supernova
1062 explosions. *The Astrophysical Journal* 450, 830.

1063 Cameron, V., Vance, D., Archer, C., House, C. H., 2009. A biomarker based on the
1064 stable isotopes of nickel. *Proceedings of the National Academy of Sciences*
1065 106 (27), 10944–10948.

1066 Ciesla, F., 2008. Radial transport in the solar nebula: Implications for moderately
1067 volatile element depletions in chondritic meteorites. *Meteoritics & Planetary*
1068 *Science* 43 (4), 639–655.

1069 Compston, W., Oversby, V., 1969. Lead isotopic analysis using a double spike.
1070 *Journal of Geophysical Research* 74, 4338–4348.

1071 Dauphas, N., Cook, D. L., Sacarabany, A., Fröhlich, C., Davis, A. M., Wadhwa,
1072 M., Pourmand, A., Rauscher, T., Gallino, R., 2008. Iron 60 Evidence for
1073 Early Injection and Efficient Mixing of Stellar Debris in the Protosolar
1074 Nebula. *The Astrophysical Journal* 686 (1), 560–569.

Dauphas, N., Marty, B., Reisberg, L., 2002a. Molybdenum Evidence for Inherited Planetary Scale Isotope Heterogeneity of the Protosolar Nebula. *The Astrophysical Journal* 565 (1), 640–644.

Dauphas, N., Marty, B., Reisberg, L., 2002b. Molybdenum nucleosynthetic dichotomy revealed in primitive meteorites. *The Astrophysical Journal, Letters* 569 (2), L139–L142.

Dauphas, N., Remusat, L., Chen, J. H., Roskosz, M., Papanastassiou, D. A., Stodolna, J., Guan, Y., Ma, C., Eiler, J. M., 2010. Neutron-rich Chromium Isotope Anomalies in Supernova Nanoparticles. *The Astrophysical Journal* 720, 1577–1591.

Davis, A., 2009. Personal communication.

Dietz, L. A., Paghugki, C. F., Land, G. A., 1962. Internal standard technique for precise isotopic abundance measurments in thermal ionization mass spectrometry. *Analytical Chemistry* 34 (6), 709–710.

Dodson, M., 1963. A theoretical study of the use of internal standards for precise isotopic analysis by the surface ionization technique: Part I- General first-order algebraic solutions. *Journal of Scientific Instruments* 40 (6), 289–295.

Dodson, M. H., 1969. A theoretical study of the use of internal standards for precise isotopic analysis by the surface ionization technique part ii: Error relationships. *Journal of Scientific Instruments* 2 (2), 490–498.

Ebel, D. S., Grossman, L., 2001. Condensation from supernova gas made of free atoms. *Geochimica et Cosmochimica Acta* 65 (3), 469–477.

Fedkin, A. V., Meyer, B. S., Grossman, L., 2010. Condensation and mixing in supernova ejecta. *Geochimica et Cosmochimica Acta* 74 (12), 3642–3658.

Gramlich, J. W., Machlan, L. A., Barnes, I. L., Paulsen, P. J., 1989a. Absolute isotopic abundance ratios and atomic weight of a reference sample of nickel. *Journal of Research of the National Institute of Standards and Technology* 94 (6), 347–356.

Gramlich, J. W., Machlan, L. A., Barnes, I. L., Paulsen, P. J., 1989b. The absolute isotopic composition and atomic weight of terestrial nickel. *Journal of Research of the National Institute of Standards and Technology* 94 (6), 357–362.

Grossman, L., Ganapathy, R., 1976a. Trace elements in the Allende meteorite–I. Coarse-grained, Ca-rich inclusions. *Geochimica et Cosmochimica Acta* 40 (3), 331–344.

Grossman, L., Ganapathy, R., 1976b. Trace elements in the Allende meteorite–II. Fine-grained. Ca-rich inclusions. *Geochimica et Cosmochimica Acta* 40 (8), 967–977.

Grossman, L., Ganapathy, R., Methot, R. L., Davis, A. M., 1979. Trace elements in the Allende meteorite–IV. Amoeboid olivine aggregates. *Geochimica et Cosmochimica Acta* 43 (6), 817–829.

Guan, Y., Huss, G., Leshin, L., 2007. ^{60}Fe-^{60}Ni and ^{53}Mn-^{53}Cr isotopic systems in sulfides from unequilibrated enstatite chondrites. *Geochimica et Cosmochimica Acta* 71 (16), 4082–4091.

Hammer, N. J., Janka, H. T., Müller, E., 2010. Three-dimensional Simulations of Mixing Instabilities in Supernova Explosions. *The Astrophysical Journal* 714, 1371–1385.

Hartmann, D., Woosley, S. E., El Eid, M. F., 1985. Nucleosynthesis in neutron-rich supernova ejecta. *The Astrophysical Journal* 297, 837–845.

Hashimoto, M., 1995. Supernova nucleosynthesis in massive stars. *Progress of Theoretical Physics* 94 (5), 663–736.

Hester, J., 2008. The crab nebula: An astrophysical chimera. *Annual Reviews in Astronomy and Astrophysics* 46, 127–155.

Heydegger, H. R., Foster, J. J., Compston, W., 1979. Evidence of a new isotopic anomaly from titanium isotopic ratios in meteoric materials. *Nature* 278 (5706), 704–707.

Hoppe, P., Leitner, J., Gröner, E., Marhas, K. K., Meyer, B. S., Amari, S., 2010. NanoSIMS studies of small presolar SiC grains: New insights into supernova nucleosynthesis, chemistry, and dust formation. *The Astrophysical Journal* 719 (2), 1370.

Ireland, T. R., 1990. Presolar isotopic and chemical signatures in hibonite-bearing refractory inclusions from the Murchison carbonaceous chondrite. *Geochimica et Cosmochimica Acta* 54 (11), 3219–3237.

1138 Iwamoto, K., Brachwitz, F., Nomoto, K., Kishimoto, N., Umeda, H., Hix, W. R.,
1139 Thielemann, F., 1999. Nucleosynthesis in chandrasekhar mass models for
1140 type IA supernovae and constraints on progenitor systems and burning-
1141 front propagation. *Astrophysical Journal, Supplement Series* 125, 439–462.

1142 Jackson, A. A., Zook, H. A., 1992. Orbital evolution of dust particles from comets
1143 and asteroids. *Icarus* 97 (1), 70–84.

1144 Jungck, M. H. A., Shimamura, T., Lugmair, G. W., 1984. Ca isotope variations in
1145 Allende. *Geochimica et Cosmochimica Acta* 48 (12), 2651–2658.

1146 Kallemeyn, G., Rubin, A., Wasson, J., 1994. The compositional classification of
1147 chondrites: VI. The CR carbonaceous chondrite group. *Geochimica et Cos-*
1148 *mochimica Acta* 58 (13), 2873–2888.

1149 Kasen, D., Röpke, F. K., Woosley, S. E., 2009. The diversity of type Ia supernovae
1150 from broken symmetries. *Nature* 460 (7257), 869–872.

1151 Kenney, J., Keeping, E., 1951. Mathematics of Statistics, Part Two, 2nd Edition.
1152 *D. Van Nostrand Company, Inc.*

1153 Kifonidis, K., Plewa, T., Janka, H.-T., Müller, E., 2003. Non-spherical core col-
1154 lapse supernovae. I. Neutrino-driven convection, Rayleigh-Taylor instabili-
1155 ties, and the formation and propagation of metal clumps. *Astronomy and*
1156 *Astrophysics* 408, 621–649.

1157 Krauss, O., Wurm, G., 2005. Photophoresis and the pile-up of dust in young
1158 circumstellar disks. *The Astrophysical Journal* 630 (2), 1088.

1159 Lee, T., Papanastassiou, D. A., Wasserburg, G. J., 1978. Calcium isotopic anoma-
1160 lies in the Allende meteorite. *The Astrophysical Journal, Letters* 220, L21–
1161 L25.

1162 Lee, T., Russell, W. A., Wasserburg, G. J., Mar. 1979. Calcium isotopic anomalies
1163 and the lack of aluminum-26 in an unusual Allende inclusion. *The Astro-*
1164 *physical Journal, Letters* 228, L93–L98.

1165 Leya, I., Schönbächler, M., Wiechert, U., Krähenbühl, U., Halliday, A. N., 2008.
1166 Titanium isotopes and the radial heterogeneity of the solar system. *Earth*
1167 *and Planetary Science Letters* 266, 233–244.

1168 Leya, I., Schönbächler, M., Krähenbühl, U, Halliday, A. N., 2009. New Titanium
1169 Isotope Data for Allende and Efremovka CAIs. *The Astrophysical Journal*
1170 702 (2), 1118—1126.

1171 Li, H., McCray, R., Sunyaev, R. A., 1993. Iron, Cobalt, and Nickel in SN 1987A.
1172 *The Astrophysical Journal* 419, 824.

1173 Liu, M.-C., McKeegan, K. D., Goswami, J. N., Marhas, K. K., Sahijpal, S., Ireland,
1174 T. R., Davis, A. M., 2009. Isotopic records in cm hibonites: Implications for
1175 timescales of mixing of isotope reservoirs in the solar nebula. *Geochimica*
1176 *et Cosmochimica Acta* 73 (17), 5051–5079.

1177 Lugaro, M., Davis, A. M., Gallino, R., Savina, M. R., Pellin, M. J., 2004. Con-
1178 straints on AGB models from the heavy-element composition of presolar
1179 SiC grains. *Memorie della Società Astronomica Italiana* 75, 723–728.

1180 Maeda, K., Röpke, F. K., Fink, M., Hillebrandt, W., Traviglio, C., Thielemann,
1181 F., 2010. Nucleosynthesis in two-dimensional delayed detonation models of
1182 type Ia supernova explosions. *The Astrophysical Journal* 712 (1), 624–638.

1183 Mahon, K., 1996. The new "York" regression: Application of an improved statisti-
1184 cal method to geochemistry. *International Geology Review* 38 (4), 293–303.

1185 Marhas, K., Amari, S., Gyngard, F., Zinner, E., Gallino, R., 2008. Iron and Nickel
1186 Isotopic Ratios in Presolar SiC Grains. *The Astrophysical Journal* 689 (1),
1187 622–645.

1188 McSween Jr., H. Y., 1977. Petrographic variations among carbonaceous chondrites
1189 of the Vigarano type. *Geochimica et Cosmochimica Acta* 41 (12), 1777–1790.

1190 Meyer, B. S., Krishnan, T. D., Clayton, D. D., 1996. ^{48}Ca production in matter
1191 expanding from high temperature and density. *The Astrophysical Journal*
1192 462, 825–839.

1193 Meyer, B. S., Weaver, T. A., Woosley, S. E., 1995. Isotope source table for a 25
1194 $M_\odot$ supernova. *Meteoritics* 30, 325–334.

1195 Moynier, F., Blichert-Toft, J., Wang, K., Herzog, G. F., Albarede, F., 2011a. The
1196 elusive ^{60}Fe in the Solar nebula. *The Astrophysical Journal* 741 (2), 71.

1197 Moynier, F., Dauphas, N., , Podosek, F. A., 2009. A search for ^{70}Zn anomalies in
1198 meteorites. *The Astrophysical Journal, Letters* 700 (2), L92–L95.

Moynier, F., Simon, J. I., Podosek, F. A., Meyer, B. S., Brannon, J., DePaolo, D. J., 2010. Ca isotope effects in orgueil leachates and the implications for the carrier phases of ^{54}Cr anomalies. *The Astrophysical Journal, Letters* 718 (1), L7.

Moynier, F., Yin, Q.-Z., Schauble, E., 2011b. Isotopic evidence of Cr partitioning into Earth's core. *Science* .

Mukai, T., Yamamoto, T., 1982. Solar wind pressure on interplanetary dust. *Astronomy and Astrophysics* 107, 97–100.

Niederer, F. R., Papanastassiou, D. A., 1984. Ca isotopes in refractory inclusions. *Geochimica et Cosmochimica Acta* 48 (6), 1279–1293.

Niederer, F. R., Papanastassiou, D. A., Wasserburg, G. J., 1980. Endemic isotopic anomalies in titanium. *The Astrophysical Journal, Letters* 240, L73–L77.

Niederer, F. R., Papanastassiou, D. A., Wasserburg, G. J., 1985. Absolute isotopic abundances of Ti in meteorites. *Geochimica et Cosmochimica Acta* 49 (3), 835–851.

Niemeyer, S., Lugmair, G. W., 1980. Ti isotope anomalies in an "un-fun" Allende inclusion. *Meteoritics* 15 (4), 341.

Nomoto, K., 1982. Accreting white dwarf models for type I supernovae. I - Presupernova evolution and triggering mechanisms. *The Astrophysical Journal* 253, 798–810.

Nomoto, K., Hashimoto, M., Tsujimoto, T., Thielemann, F. K., Kishimoto, N., Kubo, Y., Nakasato, N., 1997. Nucleosynthesis in type II supernovae. *Nuclear Physics A* 616, 79–90.

Qin, L., Nittler, L. R., Alexander, C. M. O., Wang, J., Stadermann, F. J., Carlson, R. W., 2011. Extreme ^{54}Cr-rich nano-oxides in the CI chondrite Orgueil – Implication for a late supernova injection into the Solar System. *Geochimica et Cosmochimica Acta* 75 (2), 629–644.

Quitté, G., Latkoczy, C., Schönbächler, M., Halliday, A. N., Günther, D., 2011. ^{60}Fe–^{60}Ni systematics in the eucrite parent body: A case study of Bouvante and Juvinas. *Geochimica et Cosmochimica Acta* 75 (23), 7698–7706.

Quitté, G., Markowski, A., Latkoczy, C., Gabriel, A., Pack, A., 2010. Iron-60 heterogeneity and incomplete isotope mixing in the early solar system. *The Astrophysical Journal* 720 (2), 1215–1224.

Rauscher, T., Heger, A., Hoffman, R. D., Woosley, S. E., 2002. Nucleosynthesis in Massive Stars with Improved Nuclear and Stellar Physics. *The Astrophysical Journal* 576 (1), 323–348.

Regelous, M., Elliott, T., Coath, C. D., 2008. Nickel isotope heterogeneity in the early solar system. *Earth and Planetary Science Letters* 272 (1-2), 330–338.

Robertson, H. P., 1937. Dynamical effects of radiation in the solar system. *Monthly Notices of the Royal Astronomical Society* 97, 423–438.

Rotaru, M., Birck, J., Allègre, C., 1992. Clues to early Solar System history from chromium isotopes in carbonaceous chondrites. *Nature* 358, 465–470.

Rugel, G., Faestermann, T., Knie, K., Korschinek, G., Poutivtsev, M., Schumann, D., Kivel, N., Günther-Leopold, I., Weinreich, R., Wohlmuther, M., 2009. New Measurement of the ^{60}Fe Half-Life. *Physical Review Letters* 103 (7), 1–4.

Russell, R., 1971. The Systematics of Double Spiking. *Journal of Geophysical Research* 76 (20), 4949–4953.

Russell, W., Papanastassiou, D., Tombrello, T., 1978. Ca isotope fractionation on the Earth and other Solar System materials. *Geochimica et Cosmochimica Acta* 42, 1075–1090.

Schönbächler, M., Lee, D., Rehkämper, M., Halliday, A. N., Fehr, M. A., Hattendorf, B., Günther, D., 2003. Zirconium isotope evidence for incomplete admixing of r-process components in the Solar nebula. *Earth and Planetary Science Letters* 216 (4), 467–481.

Schönbächler, M., Rehkämper, M., Fehr, M. A., Halliday, A. N., Hattendorf, B., Günther, D., 2005. Nucleosynthetic zirconium isotope anomalies in acid leachates of carbonaceous chondrites. *Geochimica et Cosmochimica Acta* 69 (21), 5113–5122.

Schönbächler, M., Rehkämper, M., Halliday, A. N., Lee, D.-C., Bourot-Denise, M., Zanda, B., Hattendorf, B., Günther, D., 2002. Niobium-zirconium chronometry and early Solar System development. *Science* 295 (5560), 1705–1708.

Shukolyukov, A., Lugmair, G. W., 2006. Manganese-chromium isotope systematics of carbonaceous chondrites. *Earth and Planetary Science Letters* 250 (1-2), 200–213.

Simon, J. I., DePaolo, D. J., Moynier, F., 2009. Calcium isotope composition of meteorites, Earth, and Mars. *The Astrophysical Journal* 702, 707–715.

Spyromilio, J., Meikle, W. P. S., Allen, D. A., 1990. Spectral line profiles of iron and nickel in supernova 1987A - Evidence for a fragmented nickel bubble. *Monthly Notices of the Royal Astronomical Society* 242, 669–673.

Steele, R. C. J., Elliott, T., Coath, C. D., Regelous, M., 2011. Confirmation of mass-independent Ni isotopic variability in iron meteorites. *Geochimica et Cosmochimica Acta* 75 (24), 7906–7925.

Tachibana, S., Huss, G. R., 2003. The initial abundance of ^{60}Fe in the Solar System. *The Astrophysical Journal* 588, L41 – L44.

Tachibana, S., Huss, G. R., K., N., 2007. ^{60}Fe-^{60}Ni Systems in ferromagnesian chondrules in least equilibrated ordinary chondrites. *Lunar and Planetary Institute Science Conference Abstracts* 38, 1709.

Tachibana, S., Huss, G. R., Kita, N. T., Shimoda, G., Morishita, Y., 2006. ^{60}Fe in chondrites: Debris from a nearby supernova in the early Solar System? *The Astrophysical Journal* 639, L87–L90.

Travaglio, C., Hillebrandt, W., Reinecke, M., Thielemann, F., 2004. Nucleosynthesis in multi-dimensional SN Ia explosions. *Astronomy and Astrophysics* 425, 1029–1040.

Trinquier, A., Birck, J.-L., Allègre, C. J., 2007. Widespread ^{54}Cr heterogeneity in the inner Solar System. *The Astrophysical Journal* 655, 1179–1185.

Trinquier, A., Birck, J. L., Allègre, C. J., Göpel, C., Ulfbeck, D., 2008. ^{53}Mn–^{53}Cr systematics of the early Solar System revisited. *Geochimica et Cosmochimica Acta* 72 (20), 5146–5163.

Trinquier, A., Elliott, T., Ulfbeck, D., Coath, C., Krot, A. N., Bizzarro, M., 2009. Origin of nucleosynthetic isotope heterogeneity in the Solar protoplanetary disk. *Science* 324 (5925), 374–376.

Umeda, H., Nomoto, K., 2002. Nucleosynthesis of zinc and iron peak elements in population III type II supernovae: Comparison with abundances of very metal poor halo stars. *The Astrophysical Journal* 565, 385–404.

Wasson, J. T., Chou, C., 1974. Fractionation of moderately volatile elements in ordinary chondrites. *Meteoritics* 9, 69–84.

Wasson, J. T., Kallemeyn, G. W., 1988. Compositions of chondrites. *Philosophical Transactions of the Royal Society of London. Series A, Mathematical and Physical Sciences* A 325, 535 – 544.

Wood, J. A., 2005. The chondrite types and their origins. In: A. N. Krot, E. R. D. Scott, & B. Reipurth (Ed.), *Chondrites and the Protoplanetary Disk*. Vol. 341 of Astronomical Society of the Pacific Conference Series. pp. 953–973.

Woosley, S. E., 1997. Neutron-rich Nucleosynthesis in Carbon Deflagration Supernovae. *The Astrophysical Journal* 476 (2), 801–810.

Wurm, G., Teiser, J., Bischoff, A., Haack, H., Roszjar, J., 2010. Experiments on the photophoretic motion of chondrules and dust aggregates—indications for the transport of matter in protoplanetary disks. *Icarus* 208 (1), 482–491.

Yokoyama, T., O'D. Alexander, C. M., Walker, R. J., 2010. Osmium isotope anomalies in chondrites: Results for acid residues and related leachates. *Earth and Planetary Science Letters* 291 (1-4), 48–59.

Yokoyama, T., Rai, V. K., Alexander, C. M. O., Lewis, R. S., Carlson, R. W., Shirey, S. B., Thiemens, M. H., Walker, R. J., 2007. Osmium isotope evidence for uniform distribution of s- and r-process components in the early Solar System. *Earth and Planetary Science Letters* 259, 567–580.

York, D., 1969. Least squares fitting of a straight line with correlated errors. *Earth and Planetary Science Letters* 5, 320–324.

York, D., Evensen, N., Martínez, M., Delgado, J., 2004. Unified equations for the slope, intercept, and standard errors of the best straight line. *American Journal of Physics* 72, 367.

Young, E. D., Galy, A., Nagahara, H., 2002. Kinetic and equilibrium mass-dependent isotope fractionation laws in nature and their geochemical and

cosmochemical significance. *Geochimica et Cosmochimica Acta* 66 (6), 1095–1104.

Zinner, E., 1998. Stellar Nucleosynthesis and the Isotopic Composition of Presolar Grains from Primitive Meteorites. *Annual Review of Earth and Planetary Sciences* 26, 147–188.

Zinner, E., 2003. Presolar grains. In: Holland, H. D., Turekian, K. K. (Eds.), *Treatise on Geochemistry*. pp. 17–39.